mathematics

MDPI

Article

Well-Balanced High-Order Discontinuous Galerkin Methods for Systems of Balance Laws

Ernesto Guerrero Fernández [1,*], Cipriano Escalante [2] and Manuel J. Castro Díaz [1]

[1] Departamento de Análisis Matemático, Estadística e Investigación Operativa y Matemática Aplicada, Facultad de Ciencias, Universidad de Málaga, 29080 Malaga, Spain; mjcastro@uma.es
[2] Departamento de Matemáticas, Campus de Rabanales, Universidad de Córdoba, 14071 Cordoba, Spain; cescalante@uco.es
* Correspondence: ernesto.guerrero@uma.es

Abstract: This work introduces a general strategy to develop well-balanced high-order Discontinuous Galerkin (DG) numerical schemes for systems of balance laws. The essence of our approach is a local projection step that guarantees the exactly well-balanced character of the resulting numerical method for smooth stationary solutions. The strategy can be adapted to some well-known different time marching DG discretisations. Particularly, in this article, Runge–Kutta DG and ADER DG methods are studied. Additionally, a limiting procedure based on a modified WENO approach is described to deal with the spurious oscillations generated in the presence of non-smooth solutions, keeping the well-balanced properties of the scheme intact. The resulting numerical method is then exactly well-balanced and high-order in space and time for smooth solutions. Finally, some numerical results are depicted using different systems of balance laws to show the performance of the introduced numerical strategy.

Keywords: systems of balance laws; exactly well-balanced; high-order methods; discontinuous Galerkin methods; ADER; Runge–Kutta; WENO; reconstruction operators

Citation: Guerrero Fernández, E.; Escalante, C.; Castro Díaz, M.J. Well-Balanced High-Order Discontinuous Galerkin Methods for Systems of Balance Laws. *Mathematics* **2022**, *10*, 15. https://doi.org/10.3390/math10010015

Academic Editor: Arturo Hidalgo

Received: 29 November 2021
Accepted: 16 December 2021
Published: 21 December 2021

1. Introduction

We consider one-dimensional systems of balance laws of the form

$$\partial_t U + \partial_x F(U) = S(U)H' + G(U). \tag{1}$$

Here, $U(x,t)$ is the state vector taking values in the space of admissibly states $\Omega \subset \mathbb{R}^M$; $F : \Omega \to \mathbb{R}^M$ is the flux; $S(U) : \Omega \to \mathbb{R}^M$, is a function that takes into account the geometrical source terms that are multiplied by the known function $H : \mathbb{R} \to \mathbb{R}$; and $G(U)$ contains algebraic source terms. We suppose that the system is hyperbolic, and therefore the jacobian matrix of the flux has M distinct real eigenvalues.

The system (1) often admits steady-state solutions that, in most cases, are non-trivial. Moreover, these solutions usually convey significant physical meaning. A paradigmatic example of this is the lake-at-rest solution of the well-known shallow-water equations. The correct preservation of these solutions plays an essential role in any simulation. Well-balanced (or exactly well-balanced) numerical schemes aim to preserve all or at least a relevant set of specific steady-state solutions up to machine precision. A precise definition of well-balanced method is given in Section 2.

An essential advantage of well-balanced schemes is that they can accurately resolve small perturbations to steady-state solutions with relatively coarse meshes. Indeed, if a numerical method cannot preserve stationary solutions or recover a stationary solution after a perturbation, the oscillations introduced may destroy the numerical solution for long integration times. Additionally, the numerical solution may be lost entirely if the perturbation is in the same order as the discretisation errors introduced by a non well-balanced method.

Then, a finer mesh or a higher-order numerical method may be considered. Still, in this case, the computational effort can quickly become excessive. The ability of the numerical scheme to correctly preserve stationary solutions becomes then a matter of paramount importance.

The first effort to preserve stationary solution was originally introduced by Bermúdez and Vázquez-Cendón in [1] for the sallow water system, where the C-property was defined as the ability of a numerical scheme to solve a set of stationary solutions exactly or, at least, with enhanced accuracy. Since then, multiple works have been published on well-balanced numerical methods [2–34]. It is of interest to highlight the recent work in [35], where the authors develop high order exactly well-balanced methods for systems of conservation laws for finite volume method with both continuous and discontinuous source terms. A similar strategy is presented in [36] for finite-difference methods. This paper extends the numerical strategy introduced within the framework of finite volume methods in [35] to Discontinuous Galerkin (DG) methods, describing a general approach to preserve stationary solutions for general systems of conservation laws.

The DG methods were introduced by Reed and Hill in [37] and were later extended to nonlinear hyperbolic systems of conservation laws by Cockburn and Shu in a series of publications [38–41]. Since then, several authors have proposed DG numerical schemes that are exactly well-balanced for a set of stationary solutions but they mainly focus on a particular system, most commonly the shallow water equations (see [42–53]).

Many hyperbolic systems of conservation laws are frequently numerically approximated with Discontinuous Galerkin methods as they allow to scale the numerical order of accuracy of the scheme quickly, thus providing an excellent resolution with coarse meshes. That makes these schemes especially well-suited when the computational effort is an important issue. A natural approach when discretising hyperbolic systems would be to use the methods of lines, in which all but the time dimension is approximated by the DG approach. The resulting time dimensional system of ODE can be then discretised using explicit methods such as Runge–Kutta [54–60]. A more sophisticated approach that allows reaching arbitrary high order in space and time in a fully implicit manner consist on ADER (Arbitrary high order DErivative Riemann problem) approach. The ADER technique was first developed by Toro and Titarev for finite volume methods [61–64] and later extended to DG methods [55,65,66]. Since then, it has been widely used in order to solve many hyperbolic systems of conservation laws see [67–72]. The recent ADER approach for DG methods is based on a predictor-corrector scheme that computes an approximated predictor solution through a fixed point algorithm locally in each element. With the DG method providing arbitrary high order in space, the combination of both techniques allows one-step fully discrete arbitrary high order in space and time numerical schemes.

The DG and ADER-DG methods have been successfully applied to geophysical flows. In the framework of the one-layer shallow water model, we highlight the work in [68–70,73] among others, and in the multilayer shallow water case in [74,75]. More recently, advances on hyperbolic reformulations of nonlinear dispersive shallow water systems that make use of the DG or ADER-DG techniques are found on [67,76–78].

A recurrent problem when high order methods are used is the appearance of spurious oscillations at discontinuities that appear when the hyperbolic system of conservation laws is considered. To avoid that, several limiting techniques exist. For instance, a multi-dimensional and optimal-order detector (MOOD) can be used (see in [79]). Alternatively, other limiter strategies are the minmod type total variation bounded (TVB) limiter [38,80], the moment-based limiter [81] and the improved moment limiter [82]. Another approach to limiting is the one based on WENO methodology, mainly developed by Shu, Qiu, and Zhu et al. (see in [83–85]). The WENO limiter approach uses a convex combination of all available neighbour polynomials, assigning essentially zero weights to stencils containing discontinuities. This work proposes a limiter procedure based on this method but takes advantage of a well-balanced reconstruction operator that preserves the well-balanced properties of the numerical method.

This paper is organised as follows. In Section 2, a brief description of the considered numerical schemes are performed, including Runge–Kutta and ADER discretisations in time. Section 3 describes the followed well-balanced methodology proposed for the numerical schemes studied. Next, in Section 4, a limiter procedure that preserves the well-balanced features of the numerical schemes is proposed. Then, in Section 5 some numerical tests are provided for the Shallow water, Burger, Euler with gravity and the hyperbolic dispersive Gavrilyuk–Favrie equations. Finally, some conclusions are given in Section 6.

2. Discontinuous Galerking Method

We briefly recall the DG method to discretise the general system (1) for one-spatial domains. We consider a set of element cells $\Omega_i = [x_{i-\frac{1}{2}}, x_{i+\frac{1}{2}}]$, with constant length Δx. The numerical solution of the PDE (1) at a given time t at each subset Ω_i is represented by $u_h(x,t)$ and is described in terms of piece-wise polynomials of degree N on the spatial direction. We shall denote by $\mathcal{U}_h$ the space of piece-wise polynomials up to degree N so that $u_h(x,t)|_{\Omega_i} \in \mathcal{U}_h$, $\forall i$.

An orthogonal nodal basis is defined by the Lagrange interpolation polynomials over the $(N+1)$ Gauss–Legendre quadrature nodes on the cell element Ω_i. We stress that the piece-wise solution u_h may be discontinuous across elements, allowing jump discontinuities at cell interfaces.

Given the element Ω_i, the discrete solution u_h projected on the nodal spatial basis polynomials $\Phi_l(x)$ reads

$$u_h(x,t) = \sum_l \hat{u}_{i,l}(t)\Phi_l(x) \coloneqq \hat{u}_{i,l}(t)\Phi_l(x), \quad \text{for } x \in \Omega_i, \tag{2}$$

with $\hat{u}_{i,l}(t)$ being the unknown degrees of freedom, and where the Einstein summation convention over two repeated indices has been considered. In this work, we suppose that $H(x)$ is a given function and it is known at every point of the domain. In the subsequent notation, we omit the space dependency of $\Phi_l(x)$ for the sake of simplicity.

The DG methods results then from multiplying the PDE system (1) with a polynomial test function $\Phi_k \in \mathcal{U}_h$ and integrating over the spatial element Ω_i. That leads to the following weak formulation where we seek $u_h(x,t) \in \mathcal{U}_h$ such that, for all Ω_i,

$$\int_{\Omega_i} \Phi_k \partial_t u_h \, dx + \int_{\Omega_i} \Phi_k \partial_x F(u_h) \, dx = \int_{\Omega_i} \Phi_k \big(S(u_h)H' + G(u_h)\big) \, dx, \tag{3}$$

holds for all test functions $\Phi_k(x) \in \mathcal{U}_h$. The dependence on x and t has been dropped for the sake of compactness. Using (2), the flux function is integrated by parts and the weak formulation (3) can be rewritten as

$$\left(\int_{\Omega_i} \Phi_k^2 \, dx\right) \frac{d}{dt}\hat{u}_{i,k} = \Phi_k(x_{i-1/2})F_{i-1/2} - \Phi_k(x_{i+1/2})F_{i+1/2} + \int_{\Omega_i^\circ} F(u_h)\Phi_k' \, dx + \int_{\Omega_i^\circ} \Phi_k \big(S(u_h)H' + G(u_h)\big) \, dx, \tag{4}$$

where the first integral contains the so-called element mass matrix, which is diagonal since the DG polynomial basis is orthogonal. Likewise, Ω_i° denotes the set of all interior points of Ω_i. The second integral accounts for the smooth part of the flux, while the last integral accounts for the presence of the continuous source terms. Finally, $F_{i-1/2} - F_{i+1/2}$ describes the jump across element interfaces given by a consistent numerical flux of the homogeneous system

$$F_{i+1/2} = \mathbb{F}\left(u^-_{h,i+1/2}, u^+_{h,i+1/2}\right), \tag{5}$$

where $u^-_{h,i+1/2}$ and $u^+_{h,i+1/2}$ are the boundary extrapolated states at the left and right of the interface $x_{i+1/2}$, respectively. Note that the numerical fluxes are multiplied by the

evaluation of the Lagrange base at the cell interfaces, $\Phi_k(x_{i\pm1/2})$. In this work, the standard HLL Riemann solver is used. However, the numerical methods described in this work can be easily extended to more accurate Riemann solvers such as the *Polynomial Viscosity Methods* or *Rational Viscosity Methods* (see [86–89]).

Definition 1. *Given a continuous stationary solution U of system (1), the semi-discrete numerical scheme (4) is said to be well-balanced (or exactly well-balanced) if the set $\{\hat{u}_{i,l} = U(x_{i,l})\}$ is an equilibrium of the ODE system, where $\{x_{i,l}\}$ is the set of nodal spatial points. Note that this definition mimics the one given in [35] or [31] for finite volume methods.*

It is clear that the semi-discrete method (4), as it is formulated, is not well-balanced in general. The following section will describe a procedure to define DG well-balanced methods.

The semi-discrete numerical scheme (4) can be then approximated with any time-marching numerical method. This work uses classical Runge–Kutta methods and the family of one-step ADER-DG methods based on a predictor-corrector scheme. In the next Subsection, a brief description of the aforementioned time discretisation methods is given. The interested reader can be referred to [38–41,80,90] for DG Runge–Kutta methods or [67–72] for ADER-DG methods.

2.1. Runge–Kutta Time Discretization

We first remark that due to the choice of an orthogonal DG polynomial basis, the mass-matrix appearing in the semi-discrete system (4) is diagonal, and that leads us to write (4) for each element Ω_i and degree of freedom $\hat{u}_{i,k}$ in the more compact form

$$\partial_t \hat{u}_{i,k}(t) = \frac{1}{\omega_k} L(\hat{u}_{i,k}(t)), \quad \omega_k = \int_{\Omega_i} \Phi_k^2 \, dx, \tag{6}$$

where $L(\hat{u}_{i,k}(t))$ is the spatial discretization operator. To discretise the time variable t, total variation diminishing (TVD) schemes have been considered in this work.

For instance, the third order Runge–Kutta scheme applied to the time interval $[t^n, t^n + \Delta t]$, Δt being the time-step, reads

$$\begin{aligned}
\hat{u}_{i,k}^{(1)} &= L(\hat{u}_{i,k}(t^n)), \\
\hat{u}_{i,k}^{(2)} &= L(\hat{u}_{i,k}(t^n) + \frac{\Delta t}{2} \hat{u}_{i,k}^{(1)}), \\
\hat{u}_{i,k}^{(3)} &= L(\hat{u}_{i,k}(t^n) - \Delta t \, \hat{u}_{i,k}^{(1)} + 2\Delta t \, \hat{u}_{i,k}^{(2)}), \\
\hat{u}_{i,k}^{n+1} &= \hat{u}_{i,k}(t^n) + \frac{\Delta t}{6} (\hat{u}_{i,k}^{(1)} + 4\hat{u}_{i,k}^{(2)} + \hat{u}_{i,k}^{(3)}).
\end{aligned} \tag{7}$$

2.2. ADER Time Discretization

The predictor-corrector ADER-DG approach leads to a high-order one-step method in both space and time. Here, the high-order accuracy in time is reached with a local space and time predictor guess. The spatial-time predictor $q_h(x,t)$ is computed based on a weak formulation of the PDE. Given the known solution $u_h(x,t^n)$ at time t^n, a Cauchy problem in the cell element is solved without considering interactions between the neighbour elements. The predictor solution is then used in (4) to compute the numerical solution $u_h(x,t^{n+1})$ at the subsequent time step.

Here, we briefly recall the numerical procedure. Given a space-time control volume $\Omega_i \times [t^n, t^{n+1}]$, the predictor solution q_h is projected onto the local space-time basis,

$$\begin{cases}
q_h(x,t) = \sum_l \theta_l(x,t)\hat{q}_l^i := \theta_l(x,t)\hat{q}_l^i, & \text{for } x \in \Omega_i, \ t \in (t^n, t^{n+1}], \\
q_h(x,t^n) = u_h(x,t^n),
\end{cases} \tag{8}$$

where again the Einstein notation has been used. If the system (1) is multiplied by the space-time test function $\theta_k \equiv \theta_k(x,t)$ and integrated over $\Omega_i \times [t^n, t^{n+1}]$, it yields

$$\int_{\Omega_i} \theta_k^{n+1} q_h(x,t^{n+1})\,dx - \int_{t^n}^{t^{n+1}} \int_{\Omega_i} \partial_t \theta_k q_h(x,t)\,dxdt = \int_{\Omega_i} \theta_k^n q_h(x,t^n)\,dx - \int_{t^n}^{t^{n+1}} \int_{\Omega_i} \theta_k \left(\partial_x F(q_h) - S(q_h)H' - G(q_h)\right) dxdt. \quad (9)$$

Using Equation (8), Equation (9) becomes a nonlinear system for the unknowns $\hat{q}_l^i$ that can be solved via a fixed point algorithm detailed in [65,91]. Notice that (9) is completely local, without any interaction with neighbouring cells. The iterative method converges in $N+1$ steps at most for linear homogeneous systems [92].

Finally, the one-step high-order in both space and time ADER-DG method, after replacing $u_h(x,t)$ by $q_h(x,t)$ in the right-hand side of (4), and integrating in the time interval $[t^n, t^{n+1}]$, reads

$$\left(\int_{\Omega_i} \Phi_k^2\,dx\right)\left(\hat{u}_{i,k}^{n+1} - \hat{u}_{i,k}^n\right) = \int_{t^n}^{t^{n+1}} \Phi_k(x_{i-1/2})F_{i-1/2} - \Phi_k(x_{i+1/2})F_{i+1/2}\,dt + \int_{t^n}^{t^{n+1}} \int_{\Omega_i^\circ} F(q_h)\partial_x \Phi_k\,dxdt + \int_{t^n}^{t^{n+1}} \int_{\Omega_i^\circ} \Phi_k \left(S(q_h)H' + G(q_h)\right) dxdt, \quad (10)$$

where

$$F_{i+1/2} = \mathbb{F}\left(q_{h,i+1/2}^-, q_{h,i+1/2}^+\right).$$

Remark 1. *DG methods are restricted to the Courant–Friedrichs–Lewy (CFL) condition*

$$\Delta t \leq \frac{CFL}{2N+1}\frac{\Delta x}{|\lambda_{max}|}, \quad CFL \in (0,1). \quad (11)$$

3. Well-Balanced Technique

In this Section, we detail a well-balanced technique for the Runge–Kutta DG methods (4)–(7) and the ADER-DG method (9) and (10).

3.1. Well-Balanced Runge–Kutta DG Methods

We propose now a spatial DG discretization method that exactly preserves stationary solutions. Later, we will discuss the well-balanced technique for the chosen time marching discretization. As in [35], we begin by computing a suited stationary solution in each element Ω_i at each time step t^n:

1. Seek for the stationary solution $u_i^*(x)$ of the minimization problem in Ω_i

$$\begin{cases} \partial_x F(u_i^*(x)) = S(u_i^*(x))H'(x) + G(u_i^*(x)),\ x \in \Omega_i & (12a) \\ \dfrac{1}{\Delta x}\displaystyle\int_{\Omega_i} u_i^*(x)\,dx = \frac{1}{\Delta x}\int_{\Omega_i} u_h(x,t^n)\,dx, & (12b) \\ \text{that minimizes } \displaystyle\int_{\Omega_i} (u_i^*(x) - u_h(x,t^n))^2\,dx. & (12c) \end{cases}$$

The previous problem is in general difficult. Nevertheless if $u_i^*(x)$ depends on a set of parameters, problem (12) reduces, in general, to a non-linear system of equations if the integrals in (12b) are approximated by quadrature formulas defined in terms of the Gaussian nodal points of the DG polynomials. Moreover, in some situations, like the ones considered below, (12a) and (12b) are enough to determine uniquely the local stationary solution. For instance, if $u_i^*(x)$ is of the form

$$u_i^*(x) = c_i + s(x),\ x \in \Omega_i,\ c_i \in \mathbb{R},\ s(x) \text{ known function}, \quad (13)$$

then the integration of (12b) by using quadrature rules leads to

$$c_i = \sum_l \omega_l (u_h(x_l, t^n) - s(x_l)), \tag{14}$$

where ω_l, x_l are the Gaussian quadrature rule weights and nodes respectively. This quadrature rule must be of the same order of the DG space approximation at the element Ω_i. Similarly, for stationary solutions $u_i^*(x)$ of the form

$$u_i^*(x) = c_i s(x),\ x \in \Omega_i,\ c_i \in \mathbb{R},\ s(x) \text{ known function}, \tag{15}$$

the constant c_i can be simply computed from (12b) and yields

$$c_i = \frac{\sum_l \omega_l u_h(x_l, t^n)}{\sum_l \omega_l s(x_l)}. \tag{16}$$

2. Compute the fluctuation DG polynomial:

$$v_{h|_{\Omega_i}}(x,t) = u_{h|_{\Omega_i}}(x,t) - u_{i,h}^*(x),\ x \in \Omega_i,\ t \in [t^n, t^{n+1}], \tag{17}$$

where $u_{i,h}^*$ is the projection of u_i^* into $\mathcal{U}_h$. Note that (12c) guarantees that $v_h(x, t^n)$ is minimal in L^2-norm.

3. To preserve stationary solutions, the numerical method (4) is modified as follows:

$$\begin{aligned}\left(\int_{\Omega_i} \Phi_k^2\, dx\right) \frac{d}{dt}\hat{u}_{i,k} = &\int_{\Omega_i^\circ} \Big(F(u_h) - F(u_{i,h}^*)\Big)\partial_x \Phi_k\, dx \\ &+ \Phi_k(x_{i-1/2})\Big(\widetilde{F}_{i-1/2} - F_{i-1/2}^*\Big) + \Phi_k(x_{i+1/2})\Big(F_{i+1/2}^* - \widetilde{F}_{i+1/2}\Big) \\ &+ \int_{\Omega_i^\circ} \Phi_k \Big(S(u_h) - S(u_{i,h}^*)\Big)\hat{H}_{i,l}\partial_x \Phi_l\, dx + \int_{\Omega_i^\circ} \Phi_k \Big(G(u_h) - G(u_{i,h}^*)\Big)\, dx,\end{aligned} \tag{18}$$

where $\hat{H}_{i,l}$ are the coordinates of the projection of $H(x)$ into $\mathcal{U}_h$, and

$$\widetilde{F}_{i+1/2} = \mathbb{F}\Big(u_i^*(x_{i+1/2}) + v_{h,i+1/2}^-, u_{i+1}^*(x_{i+1/2}) + v_{h,i+1/2}^+\Big), \tag{19}$$

is the usual first-order consistent numerical flux evaluated at the states

$$u_i^*(x_{i+1/2}) + v_{h,i+1/2}^-, \quad u_{i+1}^*(x_{i+1/2}) + v_{h,i+1/2}^+, \tag{20}$$

where u_i^* and u_{i+1}^* are the stationary solutions computed at the step 1 at cells Ω_i and Ω_{i+1}, respectively, and $v_{h,i+1/2}^- = v_{h|_{\Omega_i}}(x_{i+1/2})$ and $v_{h,i+1/2}^+ = v_{h|_{\Omega_{i+1}}}(x_{i+1/2})$ are the extrapolated values of the fluctuation computed at step 2 onto the left and right cell interfaces respectively. Finally, $F_{i+1/2}^*$ denotes the evaluation of the physical flux function at the stationary solution at the intercells:

$$F_{i+1/2}^* = F(u_i^*(x_{i+1/2})).$$

Remark 2. *The procedure to compute a stationary solution* (13)-(16) *can be generalized for some other different stationary solutions, or even for a k-parameter family of stationary solutions as described in* [35],

$$u_h^*(x; c_{i,1}, \ldots, c_{i,k}),\ c_{i,r} \in \mathbb{R}.$$

Remark 3. *We stress that, as* u_i^* *is a solution of* (12), *then* (18) *is of the same order of accuracy than* (4) *(see in* [35] *for more details).*

Theorem 1. *The semi-discrete numerical method* (18) *is well-balanced for a continuous global stationary solution* u^**, provided that every* u_i^* *defined by* (12) *verifies* $u^*_{|\Omega_i} = u_i^*$ *for each* Ω_i*, in the sense that* $\hat{u}^*_{i,k}$*, coordinates of the projection of* u^* *into* $\mathcal{U}_h$*, is an equilibrium of the ODE system* (18)*.*

Proof. We consider as initial condition $\hat{u}_{i,k}(0) = \hat{u}^*_{i,k}$, that implies

$$u_{h|_{\Omega_i}}(x,0) = u^*_{i,h}(x),\ x \in \Omega_i,$$

and the three volume integrals are zero. In the same way, the fluctuations $v_{h|_{\Omega_i}}(x,0) = u_{h|_{\Omega_i}}(x,0) - u^*_{i,h}(x) = 0$, therefore the extrapolated values onto the element interfaces, $v^-_{h,i-1/2}(0)$ and $v^+_{h,i-1/2}(0)$, are exactly zero as well. The continuity of u^* implies that $u_i^*(x_{i-1/2}) = u^*_{i-1}(x_{i-1/2}) = u^*(x_{i-1/2})$ and the consistency of the numerical flux implies that

$$\begin{aligned}
&\widetilde{F}_{i-1/2} - F^*_{i-1/2} = \\
&= \mathbb{F}\Big(u^*_{i-1,h}(x_{i-1/2}) + v^-_{h,i-1/2}(0), u^*_{i,h}(x_{i-1/2}) + v^+_{h,i-1/2}(0)\Big) - F(u_i^*(x_{i-1/2})) \\
&= \mathbb{F}(u^*(x_{i-1/2}), u^*(x_{i-1/2})) - F(u^*(x_{i-1/2})) = 0.
\end{aligned}$$

The same reasoning can be applied to prove that $F^*_{i+1/2} - \widetilde{F}_{i+1/2} = 0$. We conclude that $\hat{u}^*_{i,k}$ in an equilibrium of the ODE system given by the semi-discrete numerical method (18). □

Once the semi-discrete well-balanced method (18) has been proposed, the Cauchy problem

$$\begin{cases} \partial_t \hat{u}_{i,k} = \dfrac{1}{\omega_k}\widetilde{L}(\hat{u}_{i,k}),\ t \in [t^n, t^{n+1}] \\ \hat{u}_{i,k}(0) = \hat{u}_{i,k,0}, \end{cases} \tag{21}$$

for an autonomous ODE system has to be solved. Here $\widetilde{L}$ is given by the right-hand side of (18). Clearly, a stationary solution u_h^* is solution of (21) if and only if

$$\widetilde{L}(u_h^*) = 0. \tag{22}$$

Therefore, given a time discretization of the form

$$\hat{u}^{n+1}_{i,k} = \hat{u}^n_{i,k} + \Delta t \varphi(\hat{u}^n_{i,k}, \Delta t),$$

for (21), the final discrete method is well-balanced for the stationary solution u_h^* if and only if

$$\varphi(u_h^*, \Delta t) = 0. \tag{23}$$

Finally, it is clear that (22) implies (23) for any Runge–Kutta method as the ones considered in this work.

3.2. Well-Balanced ADER DG Methods

To design a well-balanced method based on the ADER time discretization, we follow a similar strategy as for the well-balanced DG Runge–Kutta method. Given an element Ω_i, a time-step t^n, and the known numerical solution $u_h(x, t^n)$:

1. First, we seek for the discrete stationary solution $u_i^*(x)$ of the Cauchy problem in Ω_i, as in the first step of the previous Section 3.1.

2. Then, we define the fluctuation DG polynomial v_h

$$\begin{cases} v_{h|_{\Omega_i}}(x,t) = q_{h|_{\Omega_i}}(x,t) - u^*_{i,h}(x),\ x \in \Omega_i,\ t \in (t^n, t^{n+1}], \\ q_{h|_{\Omega_i}}(x,t^n) = u_{h|_{\Omega_i}}(x,t^n),\ x \in \Omega_i, \\ v_{h|_{\Omega_i}}(x,t^n) = u_{h|_{\Omega_i}}(x,t^n) - u^*_{i,h}(x),\ x \in \Omega_i, \end{cases} \tag{24}$$

and the local space-time predictor given in (9) is modified as follows:

$$\begin{aligned} &\int_{\Omega_i} \theta_k^{n+1} v_h(x,t^{n+1})\,dx - \int_{t^n}^{t^{n+1}} \int_{\Omega_i} \partial_t \theta_k v_h(x,t)\,dxdt \\ &\quad = \int_{\Omega_i} \theta_k^n v_h(x,t^n)\,dx - \int_{t^n}^{t^{n+1}} \int_{\Omega_i} \theta_k \Big(\partial_x F(q_h) - \partial_x F(u^*_{i,h})\Big) \\ &\quad + \int_{t^n}^{t^{n+1}} \int_{\Omega_i} \theta_k \Big(\Big(S(q_h) - S(u^*_{i,h})\Big)\hat{H}_{i,l}\partial_x \Phi_l + G(q_h) - G(u^*_{i,h})\Big) \end{aligned} \tag{25}$$

Once the nonlinear system for the unknown $\hat{v}^i_l$ has been solved via a fixed point algorithm, the space-time predictor $q_h(x,t)$ is recovered as

$$q_{h|_{\Omega_i}}(x,t) = v_{h|_{\Omega_i}}(x,t) + u^*_{i,h}(x),\ x \in \Omega_i,\ t \in [t^n, t^{n+1}].$$

3. Finally, the one-step ADER-DG method described in (10) is modified as follows:

$$\begin{aligned} &\left(\int_{\Omega_i} \Phi_k^2\,dx\right)\left(\hat{u}^{n+1}_{i,k} - \hat{u}^n_{i,k}\right) = \int_{t^n}^{t^{n+1}} \int_{\Omega_i^\circ} \Big(F(q_h) - F(u^*_{i,h})\Big)\partial_x \Phi_k\,dxdt \\ &+ \int_{t^n}^{t^{n+1}} \Phi_k(x_{i-1/2})\Big(\widetilde{F}_{i-1/2}(t) - F^*_{i-1/2}\Big) + \Phi_k(x_{i+1/2})\Big(F^*_{i+1/2} - \widetilde{F}_{i+1/2}(t)\Big)\,dt \\ &+ \int_{t^n}^{t^{n+1}} \int_{\Omega_i} \Phi_k \Big(\Big(S(q_h) - S(u^*_{i,h})\Big)\hat{H}_{i,l}\partial_x \Phi_l + G(q_h) - G(u^*_{i,h})\Big)\,dxdt, \end{aligned} \tag{26}$$

where

$$\widetilde{F}_{i+1/2}(t) = \mathbb{F}\Big(u^*_i(x_{i+1/2}) + v^-_{h,i+1/2}(t), u^*_{i+1}(x_{i+1/2}) + v^+_{h,i+1/2}(t)\Big), \tag{27}$$

is the usual first order consistent numerical flux evaluated at the reconstructed predictor states

$$u^*_i(x_{i+1/2}) + v^-_{h,i+1/2}(t), \quad u^*_{i+1}(x_{i+1/2}) + v^+_{h,i+1/2}(t),$$

where u^*_i and u^*_{i+1} are the stationary solutions computed at the step 1 at cells Ω_i and Ω_{i+1}, respectively, and $v^-_{h,i+1/2}(t)$ and $v^+_{h,i+1/2}(t)$ are the extrapolated values of the fluctuation computed at step 2 onto the left and right cell interfaces, respectively. Additionally, $F^*_{i+1/2}$ denotes the evaluation of the physical flux at the local stationary solution at the inter-cells:

$$F^*_{i+1/2} = F(u^*_i(x_{i+1/2})).$$

Note that the added terms in the DG system (18) and ADER-DG system (26) are zero up to the order of the method. In this way, when the solution is far from a stationary solution, the solution yielded by these systems will be the same as their non-well-balanced counterparts (4) and (10) up to the order of the method. Additionally, in Section 5 a numerical example is given where a comparison between a well-balanced and non well-balanced simulation for a problem far from the equilibrium.

Finally, we stress that, although the techniques here have been described for the particular case of one-dimensional problems, all methods can be easily extended in a dimension by dimension fashion for the case of multiple spatial dimensions. For an

implementation of the DG method in the higher spatial dimension case, we refer the reader to the work in [76].

4. A Well-Balanced WENO Limiting Procedure

We now detail the limiting procedure employed in this work, based on Zhong and Shu's work in [83], where the authors propose a weighted essentially non-oscillatory (WENO) limiter for Runge–Kutta DG methods.

The main difference with our proposal is that we limit the fluctuations with respect to the stationary solutions, denoted by v_h, rather than the solution itself. Once the fluctuation has been limited, the numerical solution can be recovered by adding the stationary solution.

The limiter can be seen as a two-steps procedure as in [83]: in the first stage, the cells that need limiting, or troubled cells, are identified. Then, in the second step, the cells that were deemed as troubled are limited.

For both Runge–Kutta and ADER time-marching discretisation, the limiting procedure is applied a priori and only once at the beginning of each time step.

4.1. Detector of Troubled Cells

We use the TVD minmod limiter detector following ideas detailed in [41,83]. We first define

$$\bar{v}_i = \frac{1}{\Delta x} \int_{\Omega_i} v_h(x, t^n)\, dx, \tag{28}$$

where $v_h(x, t^n)$ denotes the fluctuation with respect to the discrete stationary solution $u^*_{i,h}(x)$ that has been computed as it is detailed in Section 3.1,

$$v_{h|_{\Omega_i}}(x, t^n) = u_{h|_{\Omega_i}}(x, t^n) - u^*_{i,h}(x), \quad x \in \Omega_i. \tag{29}$$

We also define

$$\widehat{v}_R = v^-_{i+\frac{1}{2}} - \bar{v}_i, \qquad \widehat{v}_L = \bar{v}_i - \tilde{v}^+_{i-\frac{1}{2}}, \tag{30}$$

where $v^+_{i-1/2}$ and $v^-_{i+1/2}$ are the evaluation of the polynomial fluctuation $v_h(x, t^n)$ onto the left and right cell interfaces respectively. Then, the minmod is applied as follows:

$$\sigma_R = \text{minmod}\big(\widehat{v}_R, \Delta^+ v_i, \Delta^- v_i\big), \qquad \sigma_L = \text{minmod}\big(\widehat{v}_L, \Delta^+ v_i, \Delta^- v_i\big), \tag{31}$$

where

$$\Delta^+ v_i = \bar{v}_{i+1} - \bar{v}_i, \qquad \Delta^- v_i = \bar{v}_i - \bar{v}_{i-1}, \tag{32}$$

and the following minmod functions are given by

$$\text{minmod}(a, b, c) = \begin{cases} a & \text{if } |a| \leq M\Delta x, \\ \text{m}(a, b, c) & \text{otherwise,} \end{cases} \tag{33}$$

$$\text{m}(a, b, c) = \begin{cases} s \min(a, b, c) & \text{if } s = \text{sign}(a) = \text{sign}(b) = \text{sign}(c), \\ 0 & \text{otherwise.} \end{cases} \tag{34}$$

Here, M is a parameter to be properly chosen depending on the PDE system. Finally, a cell is marked as troubled if $\text{minmod}(a, b, c) \neq a$.

4.2. Limiting Procedure

The limiting technique for the cells marked as troubled by the detector described in the previous Subsection is now detailed. The general idea is to reconstruct a new polynomial solution at a troubled cell as a convex combination of its neighbouring polynomials.

If the cell Ω_i is deemed troubled, then the first step consist on projecting the fluctuation at each neighbour element $\Omega_j,\ j \in \{i-1, i, i+1\}$, into a first-order DG polynomial with the following form:

$$v_{p,j}(x) = \frac{1}{\Delta x}\int_{\Omega_j} v_{j,h}(x)\,dx + \frac{(x - x_{j,c})}{\Delta x}\int_{\Omega_j}\frac{\partial}{\partial_x} v_{j,h}(x)\,dx,\ x \in \Omega_j, \tag{35}$$

that is a first order polynomial that preserves the cell average of $v_{j,h}(x)$. Here, the sub-index p denotes the projected polynomial using (35). We remark that we have used again v_h to denote the fluctuation with respect to the stationary solution as in (29). Likewise, $x_{j,c}$ denotes the centre of the element Ω_j and the time dependency has been dropped to simplify the notation.

This projected polynomial is then used to rewrite the new polynomial fluctuation on the element Ω_i as follows:

$$v_{h|_{\Omega_i}}^{(\text{new})}(x) = \omega_{0,i}\overline{v}_{i-1,p}(x) + \omega_{1,i}v_{i,p}(x) + \omega_{2,i}\overline{v}_{i+1,p}(x), \quad x \in \Omega_i, \tag{36}$$

where

$$\overline{v}_{i\pm1,p}(x) = v_{i\pm1,p}(x) - \frac{1}{\Delta x}\int_{\Omega_i} v_{i\pm1,p}(x)\,dx + \frac{1}{\Delta x}\int_{\Omega_i} v_{i,h}(x)\,dx, \tag{37}$$

which ensures that $v_{h|_{\Omega_i}}^{(\text{new})}(x)$ has the same cell average as $v_{h|_{\Omega_i}}(x)$. As we have made use of the fluctuation to calculate the new limited solution, the final limited solution is computed as

$$u_{h|_{\Omega_i}}^{(\text{new})}(x) = u_{i,h}^{*}(x) + v_{h|_{\Omega_i}}^{(\text{new})}(x). \tag{38}$$

The normalized weights for the WENO convex combination in (36) follows the classical WENO procedure:

$$\omega_{l,i} = \frac{\bar{\omega}_{l,i}}{\bar{\omega}_{0,i} + \bar{\omega}_{1,i} + \bar{\omega}_{2,i}}, \quad \bar{\omega}_{l,i} = \frac{\gamma_l}{(\epsilon + \beta_l)^r}, \quad l = 0, 1, 2. \tag{39}$$

The parameters γ_l used in this paper are $\gamma_1 = 0.998$, and $\gamma_{0,2} = 0.001$; ϵ is set to $\epsilon = 10^{-6}$. The employed values for r are in $\{0.25, 2\}$, and will be better detailed in the next Subsection. Finally, the smooth indicators $\beta_{l,i}$ are defined as

$$\beta_{l,i} = \sum_{s=1}^{2}\int_{\Omega_i}\Delta x^{2s-1}\left(\frac{\partial^s}{\partial x^s}v_{p,l}(x)\right)^2 dx. \tag{40}$$

Again, we stress that the general limiting procedure described here is applied once per time-step for either Runge–Kutta or ADER time discretisation.

4.3. Double-Loop Limiting Procedure

Even though the component-wise WENO technique is essentially non-oscillatory, the resulting scheme may still generate spurious oscillations, especially at very high order. We, therefore, propose the following strategy.

- First, the procedure (35)–(38) with the value $r = 2$ is used to produce a candidate solution $u_h^c(x)$. This candidate solution is evaluated once more by the detector described in Section 4.1.
- Then, if the element is once again considered as troubled, the limiting strategy (35)–(38) will be repeated changing the projector operator. Now, the fluctuation is projected into a constant value given by

$$v_{j,p}(x) = \frac{1}{\Delta x}\int_{\Omega_j} v_{j,h}(x)\,dx. \tag{41}$$

Additionally, the parameter r will be set to $r = 0.25$. This strategy will ensure a smoother discrete solution for highly oscillating regions near strong discontinuities.

That finishes the limiting technique description.

Remark 4. *It is essential to notice that the stationary solutions considered in this work are smooth, and therefore the detector does not mark cells as troubled. However, let us suppose that roundoff errors or local extremes provoke that an element is marked as troubled in the presence of a stationary solution. In that case, the use of the fluctuation* (29) *will ensure that the stationary solution is preserved, since the procedure* (35)–(38) *is exact for the null operator.*

5. Numerical Test

In this Section, some numerical experiments are conducted to test the proposed numerical first, second, third and fourth-order schemes for Runge–Kutta and ADER time discretisations.

We consider four systems: Burgers, Shallow water, Euler with gravity and the hyperbolic dispersive Gavrilyuk–Favrie equations. For each system, a brief description is given. Then, we test the ability of the numerical scheme to preserve stationary solutions. Afterwards, some numerical tests consisting of a perturbation of a stationary solution are shown alongside the behaviour of the well-balanced limiter technique proposed in this paper.

The CFL number in (11) is always set to 0.9, meanwhile the limiter value M defined in (33) is set to 1, except for the problem (63) that is set to 0.1. For the rest of the limiter parameters appearing in Section 4, we maintain the same values that were defined in that Subsection.

Remark that for the two-spatial domain dispersive system, the CFL condition (11) for DG methods in the case of two dimensional domains reads

$$\Delta t \leq \frac{1}{2}\frac{CFL}{2N+1}\frac{\min\{\Delta x, \Delta y\}}{|\lambda_{max}|}, \quad CFL \in (0,1),$$

and we set $CFL = 0.9$. Besides, for the two dimensional system, the values of the γ weights for the limiter are set to $\gamma_c = 0.996$ for the central element, and $\gamma = 0.001$ for the four neighbouring elements.

5.1. Burgers' Equation

Let us consider the one-dimensional scalar balance law consisting of Burgers' equation with a source term written in the form (1) with

$$U = u, \quad F(U) = \frac{u^2}{2}, \quad S(U) = u^2, \quad G(U) = 0, \tag{42}$$

whose stationary solutions are given by

$$u(x) = Ce^{H(x)}, \quad C \in \mathbb{R}, \tag{43}$$

and with $H(x)$ a known continuous function.

5.1.1. Preservation of a Stationary Solution

In this numerical experiment we set as initial condition a stationary solution of the form (43) to ensure the well-balancing properties of the proposed methods for the system (42). The initial condition considered is given by

$$u = e^{H(x)}, \quad H = x. \tag{44}$$

The computational domain is $\Omega = [-1, 1]$. Dirichlet and open boundary conditions were imposed at the left and at the right of the domain, respectively. Figure 1 shows the

error between the computed numerical solutions and the stationary one given by $e^{H(x)}$. As it can be seen in Figure 1 and Table 1, the well-balanced methods can preserve the stationary solution at a final time $t = 10$ s.

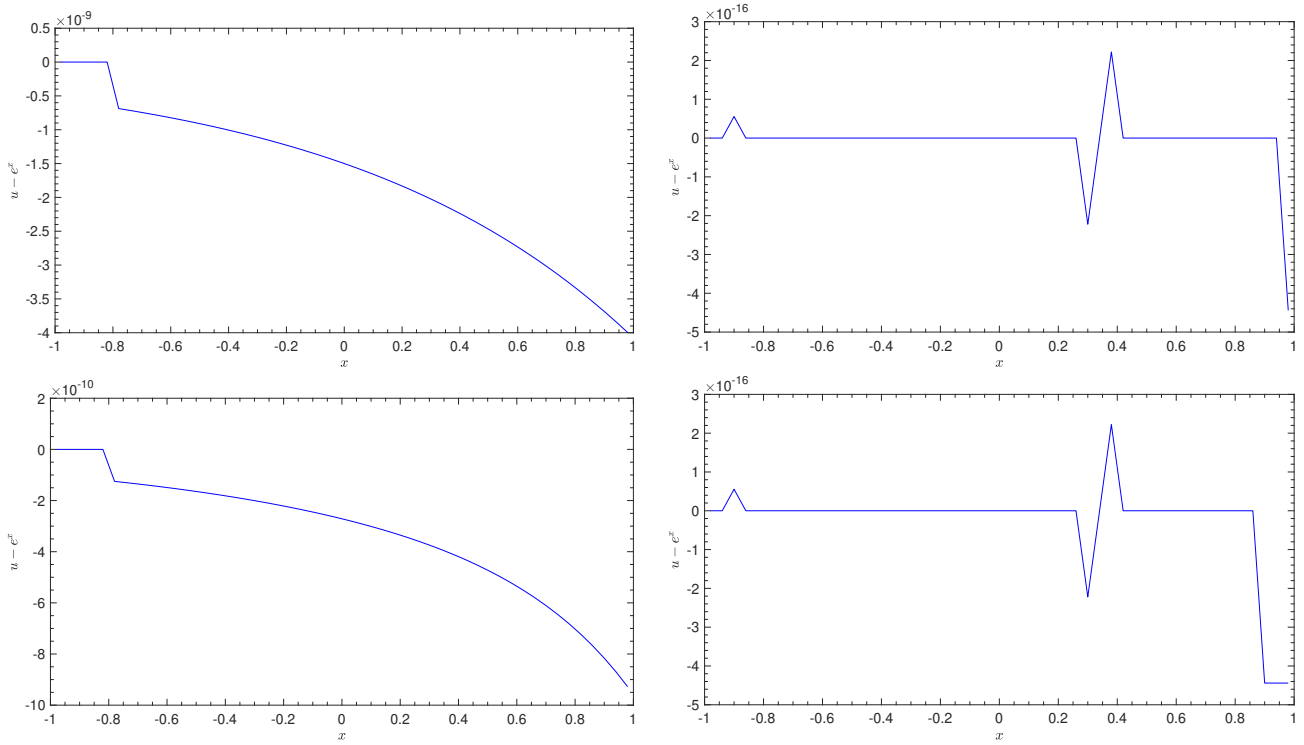

Figure 1. Fluctuation $(u - e^H)$ for the stationary problem (44) for the Burgers' equation at time $t = 10$ s with the fourth order non well-balanced (**left**) and well-balanced (**right**) numerical schemes. An uniform Cartesian mesh of $N_x = 50$ elements has been used. Upper and lower panels stands for Runge–Kutta and ADER time-marching discretisations, respectively.

Table 1. Numerical validation of the well-balanced and non well-balanced methods for the stationary problem (44) (Burgers' equation). Table contains L_1 errors for the variable u at a final time $t = 10$ s for both Runge–Kutta and ADER DG schemes of order $N + 1 = 1, 2, 3, 4$. Uniform Cartesian meshes of N_x elements has been used.

		Non Well-Balanced		**Well-Balanced**	
N	N_x	**Runge-Kutta**	**ADER**	**Runge-Kutta**	**ADER**
0	25	1.39×10^{-01}	1.39×10^{-01}	0	0
	50	6.52×10^{-02}	6.52×10^{-02}	2.66×10^{-17}	0
	100	3.17×10^{-02}	3.17×10^{-02}	1.55×10^{-17}	0
	200	1.56×10^{-02}	1.56×10^{-02}	0	0
1	25	6.47×10^{-04}	5.37×10^{-04}	8.88×10^{-18}	0
	50	1.60×10^{-04}	1.34×10^{-04}	0	0
	100	3.96×10^{-05}	3.33×10^{-05}	2.22×10^{-18}	1.11×10^{-18}
	200	9.85×10^{-06}	8.29×10^{-06}	2.22×10^{-18}	5.55×10^{-19}
2	25	4.49×10^{-06}	3.80×10^{-06}	0	2.47×10^{-18}
	50	5.91×10^{-07}	5.25×10^{-07}	7.40×10^{-18}	0
	100	7.57×10^{-08}	6.85×10^{-08}	2.47×10^{-18}	0
	200	9.57×10^{-09}	8.75×10^{-09}	1.23×10^{-18}	9.25×10^{-19}
3	25	2.56×10^{-08}	1.10×10^{-08}	4.63×10^{-18}	3.09×10^{-18}
	50	1.70×10^{-09}	7.85×10^{-10}	1.54×10^{-18}	7.53×10^{-18}
	100	1.09×10^{-10}	5.61×10^{-11}	2.32×10^{-18}	4.15×10^{-18}
	200	6.91×10^{-12}	4.00×10^{-12}	1.54×10^{-18}	2.27×10^{-18}

5.1.2. Perturbed Stationary Solutions

We consider now a perturbation of the stationary solution (44) given by

$$u = e^H + 0.3e^{-200(x+0.5)^2}, \quad H = x. \tag{45}$$

The computational domain $\Omega = [-1, 1]$ is covered with a coarse mesh of $N_x = 100$ elements. Dirichlet and open boundary conditions are imposed at the left and the right of the domain, respectively. The numerical experiment is run up to time $t = 10$ s with the fourth-order DG method and for both Runge–Kutta and ADER time discretisations.

Figure 2 shows the error between the computed numerical solutions and the stationary one given by e^H. As it can be seen, once the perturbation has left the domain, the well-balanced numerical scheme is able to recover the stationary solution e^H, in contrast with the non well-balanced scheme.

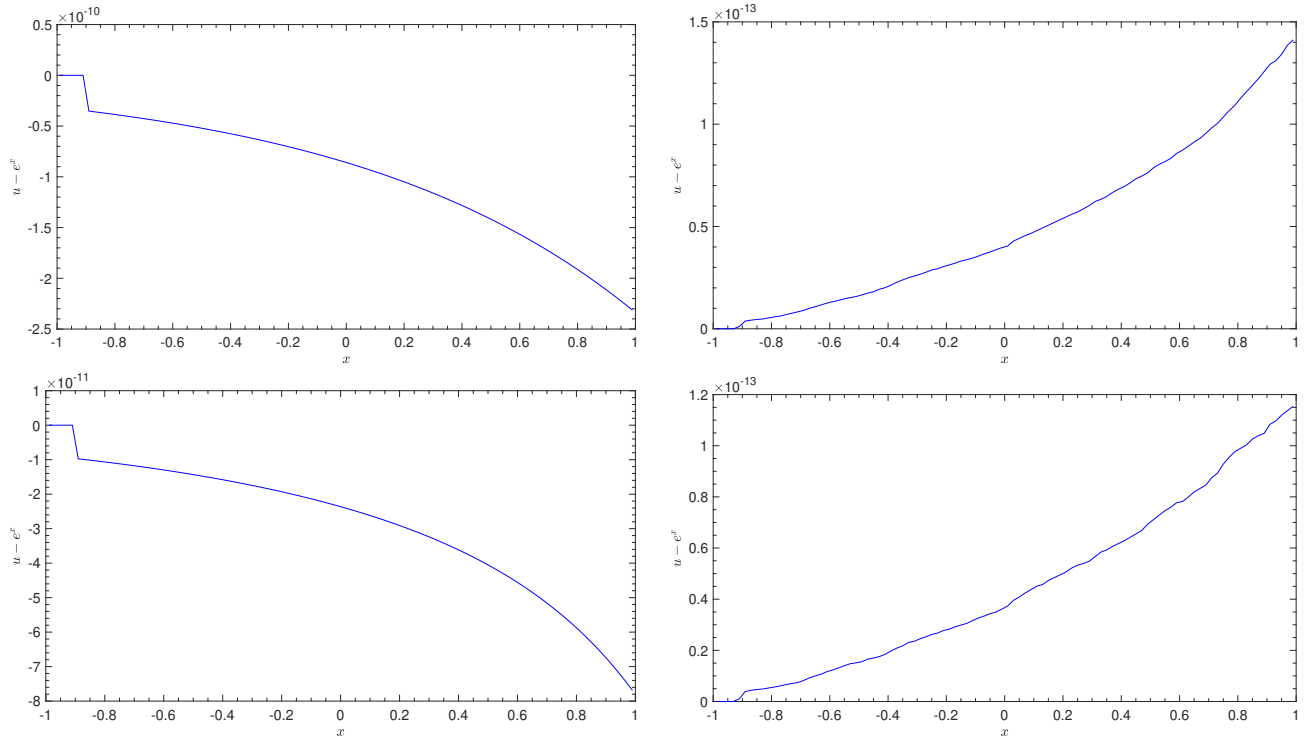

Figure 2. Fluctuation with respect to the stationary solution $(u - e^H)$ (45) for the Burgers' equation at time $t = 10$ s with the fourth order non well-balanced (**left**) and well-balanced (**right**) methods. An uniform Cartesian mesh of $N_x = 100$ elements has been used. Upper and lower panels stands for Runge–Kutta and ADER time marching discretisations respectively.

5.1.3. Limited Simulation

In this final example, we aim to check the robustness of the proposed limiter technique described in this paper. To do that, we consider the initial condition

$$u = \frac{1}{2} + \sin(x), \quad H = 0. \tag{46}$$

The computational domain $\Omega = [0, 2\pi]$ is covered with a coarse mesh of $N_x = 80$ elements. Periodic boundary conditions were imposed everywhere. Figure 3 shows the numerical approximation of u with different time-marching discretisations at the final time $t = 1.5$ s, as well as a reference solution that has been computed by a first order scheme with $N_x = 20{,}000$ elements. As it can be seen, the proposed schemes provide an accurate approximation without producing any spurious oscillations, even for the case of coarse meshes.

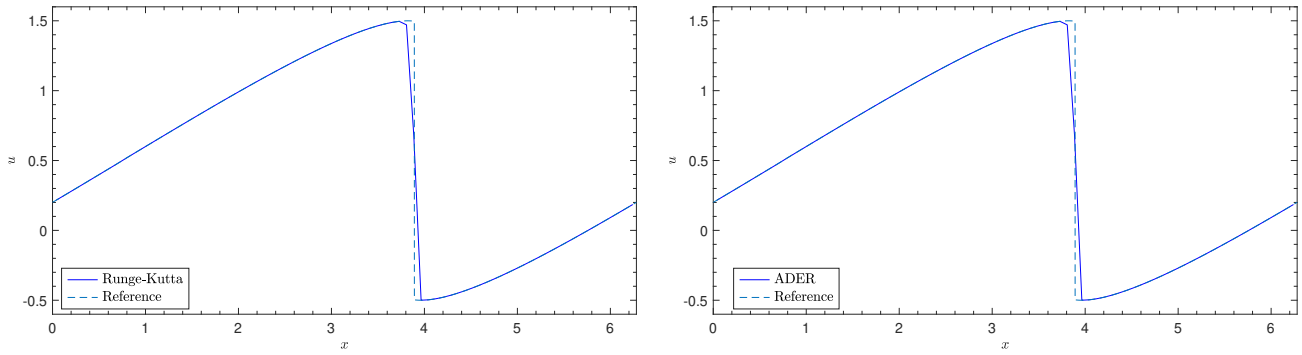

Figure 3. Computed variable u for the problem (46) (Burgers' equation) with the fourth-order well-balanced Runge–Kutta (**left**) and ADER (**right**) numerical methods at time $t = 1.5$ s. An uniform Cartesian mesh of $N_x = 80$ elements has been used.

5.1.4. Well-Balanced and Non-Well-Balanced Schemes Comparison

We perform now a comparison between the well-balanced and non-well-balanced schemes for a solution which is not a perturbation of an equilibrium state. Particularly, the following initial condition is considered:

$$u = 0.1e^{-200(x+0.5)^2}, \quad H = x. \tag{47}$$

Periodic boundary conditions and 100 discretization points are considered in a computational domain $\Omega = [-1, 1]$. Figure 4 depicts the results for a Runge–Kutta second and third order scheme. The reference solution has been computed using a first order method with 20,000 discretization points. As it can be seen, the results shows that the well-balanced and non well-balanced methods are in fact very similar regardless of the order of the method. Similar results are obtained for ADER time marching methods.

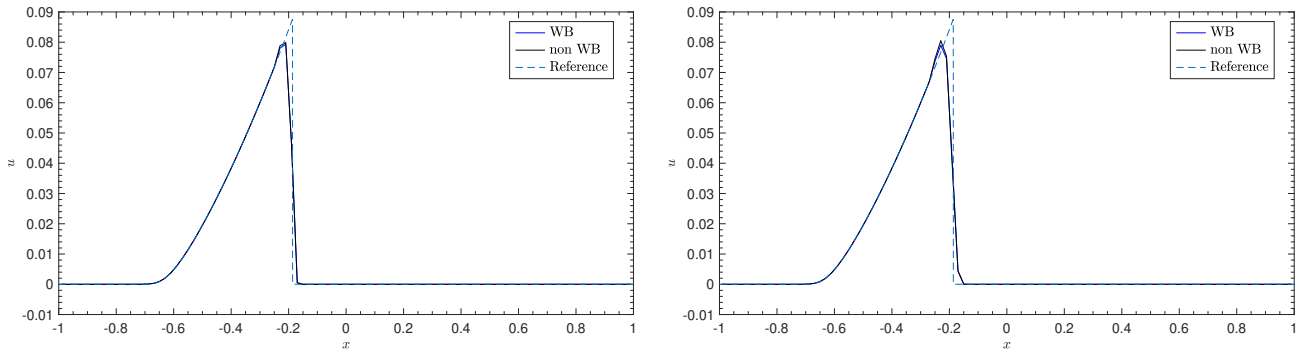

Figure 4. Computed variable u for the problem (47) (Burgers' equation) with the second (**left**) and third (**right**) order well-balanced Runge–Kutta numerical methods at time $t = 5$ s. An uniform Cartesian mesh of $N_x = 100$ elements has been used.

5.2. Shallow Water Equations

Let us consider the one-dimensional shallow water equations written in the form (1) with

$$U = \begin{pmatrix} h \\ hu \end{pmatrix}, \quad F(U) = \begin{pmatrix} hu \\ hu^2 + \frac{1}{2}gh^2 \end{pmatrix}, \quad S(U) = \begin{pmatrix} 0 \\ gh \end{pmatrix}, \quad G(U) = 0, \tag{48}$$

where $h = h(x,t)$ is the total water depth, u is the depth-averaged velocity on the $x-$direction, and $H = H(x)$ is the known still water depth that we will suppose to be continuous. Finally, $g = 9.81$ is the gravitational acceleration. In this case we adapt the well-

balanced strategy described in Section 3 to preserve the stationary solutions corresponding to water at rest:

$$u = 0, \quad \eta = cst, \tag{49}$$

where $\eta = h - H$ is the free-surface elevation.

A well-balance method could also be design following the ideas described in [93].

5.2.1. Order of Accuracy Test

We begin by checking numerically the order of accuracy of the numerical scheme for a Runge–Kutta and ADER time discretisation for a second-, third-, and fourth-order schemes. As pointed before, we consider here only a well-balanced method that preserves the water at rest solution adapting the strategy described in Section 3. The computational domain is $\Omega = [-5, 5]$, and periodic boundary conditions are imposed everywhere. We then simulate the propagation of a Gaussian wave, with the initial condition given by

$$u = 0, \quad h = H + 0.1e^{-x^2}, \quad H = 1 - 0.2e^{-x^2}, \tag{50}$$

and until the final time $t = 1$ second, with a set of refined meshes. Table 2 shows the L_1 errors and the numerical convergence rates. The expected convergence order of the Runge–Kutta and ADER DG methods can be observed.

Table 2. Numerical convergence results for the initial condition (50) (shallow water equations). High-order Runge–Kutta and ADER DG schemes of order $N + 1 = 2,\ 3,\ 4$. Uniform Cartesian meshes of N_x elements has been used. The L_1 errors refer to the variables h and hu at a final time $t = 1$ s.

		Runge-Kutta				**ADER**			
		h		***hu***		***h***		***hu***	
N	N_x	**Error**	**Order**	**Error**	**Order**	**Error**	**Order**	**Error**	**Order**
1	25	3.93×10^{-03}	-	1.27×10^{-02}		3.60×10^{-03}	-	1.17×10^{-02}	-
	50	5.92×10^{-04}	2.73	1.86×10^{-03}	2.77	8.91×10^{-04}	2.01	2.79×10^{-03}	2.07
	100	1.11×10^{-04}	2.41	3.49×10^{-04}	2.41	2.21×10^{-04}	2.01	6.78×10^{-04}	2.04
	200	2.16×10^{-05}	2.37	6.81×10^{-05}	2.36	5.50×10^{-05}	2.00	1.67×10^{-04}	2.02
2	25	7.37×10^{-05}	-	2.19×10^{-04}	-	2.97×10^{-04}	-	9.46×10^{-04}	-
	50	3.27×10^{-06}	4.49	9.72×10^{-06}	4,50	3.28×10^{-05}	3.18	1.06×10^{-04}	3.15
	100	2.47×10^{-07}	3.73	7.30×10^{-07}	3.74	3.79×10^{-06}	3.11	1.26×10^{-05}	3.08
	200	2.23×10^{-08}	3.47	6.92×10^{-08}	3.40	4.60×10^{-07}	3.04	1.55×10^{-06}	3.02
3	25	3.52×10^{-06}	-	1.02×10^{-05}	-	9.48×10^{-06}	-	3.43×10^{-05}	-
	50	1.41×10^{-07}	4.64	3.52×10^{-07}	4.86	6.60×10^{-07}	3.84	2.24×10^{-06}	3.94
	100	8.95×10^{-09}	3.98	2.21×10^{-08}	3.99	4.41×10^{-08}	3.91	1.44×10^{-07}	3.96
	200	5.63×10^{-10}	3.99	1.39×10^{-09}	3.99	2.75×10^{-09}	4.00	9.12×10^{-09}	3.98

5.2.2. Preserving Stationary Solutions

In this experiment, we set as initial condition a stationary solution of the form (49) to ensure that the well-balanced methods are able to preserve it up to machine precision, while the non well-balanced methods fail. The initial condition considered is given by

$$u = 0, \quad h = H, \quad H = 1 - 0.8e^{-100x^2}. \tag{51}$$

The computational domain is $\Omega = [-1, 1]$ and Dirichlet boundary conditions are imposed everywhere. As it can be seen in Figure 5 and Tables 3 and 4, the well-balanced methods are able to preserve the stationary solution at a final time $t = 10$ s for both time-marching discretisations and relative coarse meshes. Again, the numerical solutions are compared with the stationary solution (51) as reference.

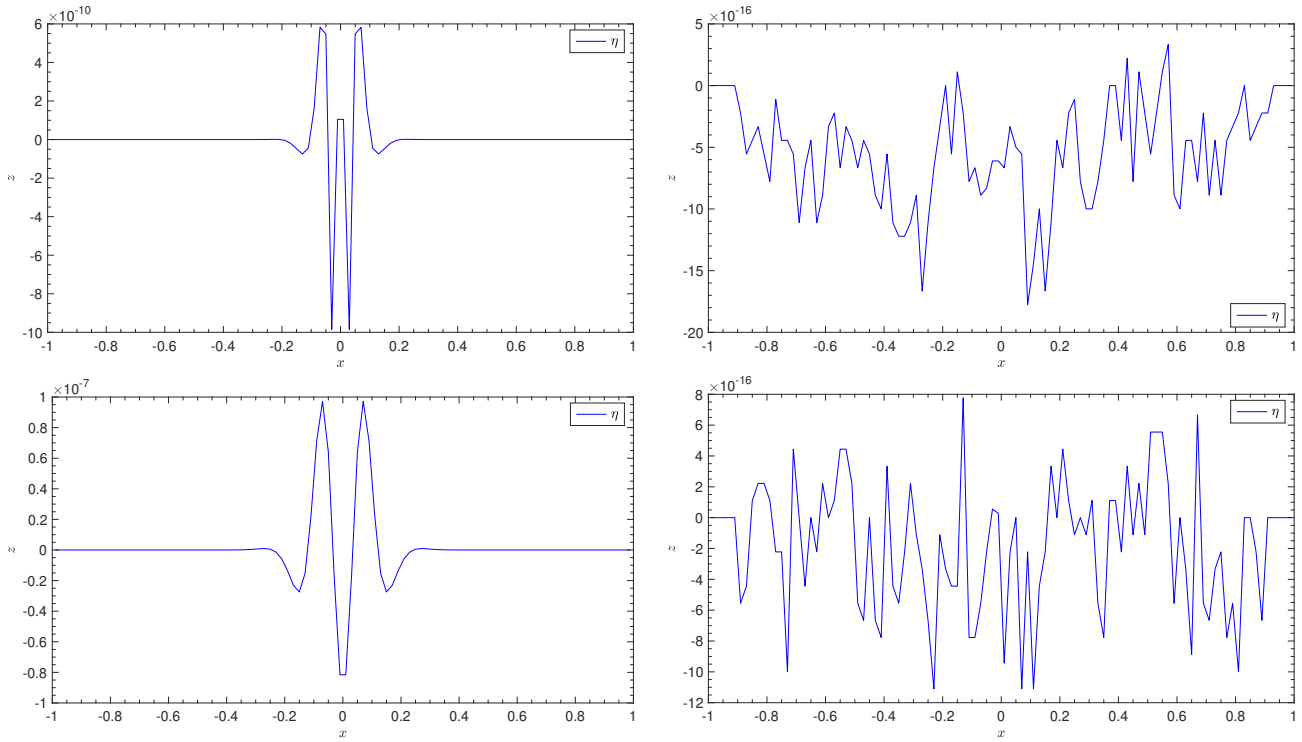

Figure 5. Computed free surface for the stationary problem (51) (sallow-water equations) at time $t = 10$ s with the fourth order non well-balanced (**left**) and well-balanced (**right**) methods. An uniform Cartesian mesh of $N_x = 100$ elements has been used. Upper and lower panels stands for Runge–Kutta and ADER time-marching discretisations respectively.

Table 3. Numerical validation of the well-balanced and non well-balanced methods for the stationary problem (51) (shallow water equations). Table contains L_1 errors for the water depth variable h at a final time $t = 10$ s for Runge–Kutta and ADER DG schemes of order $N + 1 = 1, 2, 3, 4$. Uniform Cartesian meshes of N_x elements has been used.

		Non-Well-Balanced		Well-Balanced	
N	N_x	Runge–Kutta	ADER	Runge-Kutta	ADER
0		1.92×10^{-02}	1.92×10^{-02}	3.00×10^{-17}	3.00×10^{-17}
		6.08×10^{-03}	6.08×10^{-03}	1.27×10^{-16}	3.34×10^{-16}
		1.40×10^{-03}	1.40×10^{-03}	4.86×10^{-17}	1.64×10^{-17}
		5.37×10^{-04}	5.32×10^{-04}	5.97×10^{-18}	2.30×10^{-17}
1		1.16×10^{-03}	2.62×10^{-03}	6.66×10^{-17}	6.88×10^{-16}
		2.73×10^{-04}	3.47×10^{-04}	2.06×10^{-16}	8.61×10^{-16}
		3.76×10^{-05}	5.48×10^{-05}	2.82×10^{-16}	1.42×10^{-15}
		4.81×10^{-06}	8.48×10^{-06}	4.37×10^{-16}	1.61×10^{-15}
2		3.22×10^{-04}	4.09×10^{-04}	1.52×10^{-16}	1.36×10^{-16}
		3.20×10^{-05}	4.39×10^{-05}	1.85×10^{-16}	1.20×10^{-15}
		2.36×10^{-06}	4.47×10^{-06}	2.74×10^{-16}	1.58×10^{-15}
		1.51×10^{-07}	4.95×10^{-07}	3.67×10^{-16}	1.96×10^{-15}
3		1.84×10^{-05}	4.18×10^{-05}	1.47×10^{-16}	1.63×10^{-15}
		1.64×10^{-06}	2.42×10^{-06}	3.11×10^{-16}	2.50×10^{-15}
		6.43×10^{-08}	6.25×10^{-08}	5.78×10^{-16}	4.14×10^{-16}
		2.08×10^{-09}	3.57×10^{-09}	6.75×10^{-16}	6.98×10^{-16}

Table 4. Numerical validation of the well-balanced and non well-balanced methods for the stationary problem (51) (shallow water equations). Table contains L_1 errors for the conserved variable hu at a final time $t = 10$ s for Runge–Kutta and ADER DG schemes of order $N + 1 = 1, 2, 3, 4$. Uniform Cartesian meshes of N_x elements has been used.

		Non-Well-Balanced		Well-Balanced	
N	N_x	Runge–Kutta	ADER	Runge–Kutta	ADER
0		6.12×10^{-02}	6.12×10^{-02}	4.40×10^{-15}	4.39×10^{-15}
		3.96×10^{-02}	3.96×10^{-02}	1.06×10^{-15}	1.11×10^{-15}
		2.20×10^{-02}	2.21×10^{-02}	4.09×10^{-16}	3.52×10^{-16}
		1.20×10^{-02}	1.20×10^{-02}	1.69×10^{-16}	1.79×10^{-16}
1		3.56×10^{-03}	6.49×10^{-03}	5.68×10^{-16}	1.07×10^{-14}
		3.35×10^{-04}	7.43×10^{-04}	5.33×10^{-16}	2.19×10^{-15}
		2.28×10^{-05}	1.38×10^{-04}	8.28×10^{-16}	9.95×10^{-15}
		1.44×10^{-06}	3.38×10^{-05}	1.30×10^{-15}	3.89×10^{-15}
2		5.27×10^{-04}	7.48×10^{-04}	3.97×10^{-16}	4.50×10^{-16}
		1.40×10^{-04}	1.82×10^{-04}	6.83×10^{-16}	4.28×10^{-15}
		1.96×10^{-05}	2.69×10^{-05}	7.47×10^{-16}	4.23×10^{-15}
		2.52×10^{-06}	3.45×10^{-06}	9.91×10^{-16}	2.79×10^{-15}
3		1.23×10^{-04}	3.02×10^{-04}	3.62×10^{-16}	1.51×10^{-14}
		2.59×10^{-06}	1.02×10^{-05}	7.01×10^{-16}	4.29×10^{-15}
		4.85×10^{-08}	3.25×10^{-07}	9.93×10^{-16}	1.08×10^{-15}
		7.75×10^{-10}	2.20×10^{-08}	1.87×10^{-15}	1.55×10^{-15}

5.2.3. Perturbed Stationary Solutions

We consider now a perturbation of the stationary solution (51) given by

$$u = 0, \quad h = 0.1e^{-100x^2} + H, \quad H = 1 - 0.8e^{-100x^2}. \tag{52}$$

The computational domain $\Omega = [-1, 1]$ is covered with $N_x = 100$ elements. Dirichlet and free-outflow boundary conditions are imposed at the right and the left of the domain, respectively.

As it can be seen in Figure 6, the well-balanced scheme can recover the stationary solution at a final time $t = 10$ s with the fourth-order DG method and for both Runge–Kutta and ADER time discretisations. In this case, we plot the difference between the numerically computed free surfaces and the exact stationary (51), which is zero.

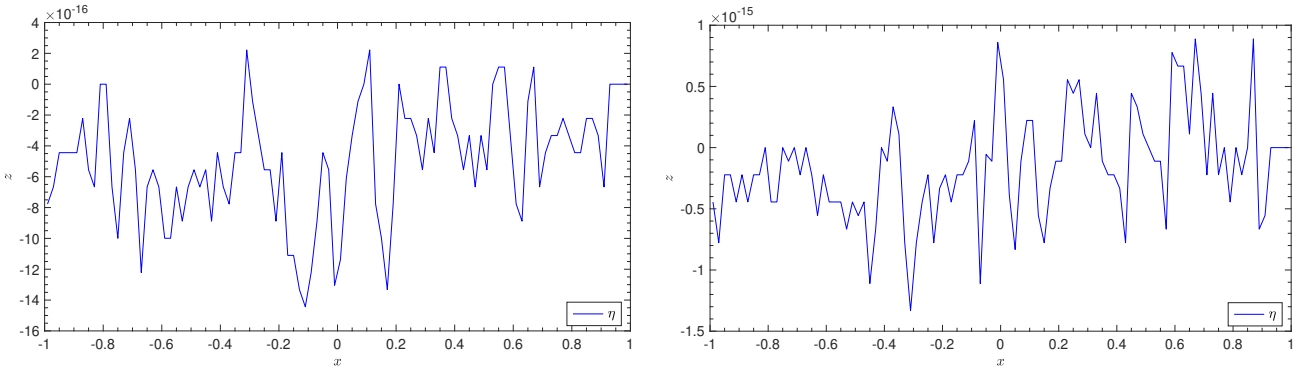

Figure 6. Computed free surface of the perturbed stationary solution (52) (sallow-water equations) with the fourth order well-balanced Runge–Kutta (**left**) and ADER (**right**) DG schemes at $t = 10$ s. A uniform Cartesian mesh of $N_x = 100$ elements has been used.

Moreover, in order to show the better performance of a well-balanced method against a non well-balanced method, we propose a similar numerical test on a very coarse mesh composed by 20 elements. Here, we consider the initial condition given by

$$u = 0, \quad h = 10^{-4} e^{-100x^2} + H, \quad H = 1 - 0.8 e^{-100x^2}. \tag{53}$$

The numerical computation is then run up to the short time $t = 0.5$ s; the perturbation does not reach boundaries in this case, and therefore periodic boundary conditions were imposed everywhere.

As the perturbation is of the order $(\Delta x)^{N+1}$, $N + 1 = 4$ being the order of the scheme, we can expect that only the well-balanced method yields satisfactory results. In contrast, the non well-balanced scheme introduces oscillations of that order that destroy the solution. Here we only show the numerical results in Figure 7 for the Runge–Kutta time discretisation. Similar results can be observed for ADER time discretisations.

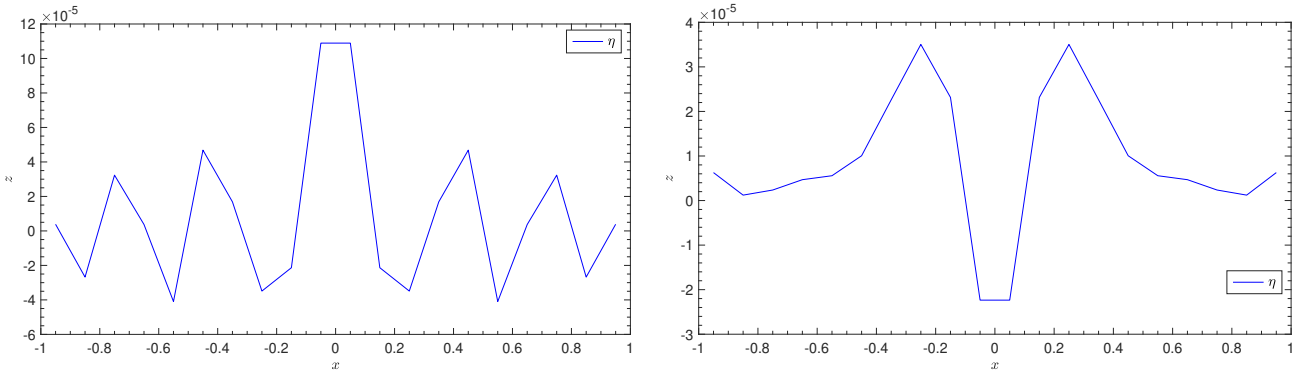

Figure 7. Computed free surface of the smaller perturbed stationary solution (53) (sallow-water equations) with the fourth order non well-balanced (**left**) and well-balanced (**right**) Runge–Kutta DG method at $t = 0.5$ s. A coarse uniform Cartesian mesh of $N_x = 20$ elements has been used.

5.2.4. Limited Simulation

In order to check the robustness of the limiting procedure described in Section 4.3, we consider now a situation far from the equilibrium, where the use of some limiting technique is mandatory. The computational domain $\Omega = [-5, 5]$ is covered now with a very refined mesh of $N_x = 400$ elements. The initial condition is set to

$$u = 0, \quad h = 0.1e^{-5x^2} + H, \quad H = 1 - 0.8e^{-x^2}. \tag{54}$$

Periodic boundary conditions are imposed to obtain more interactions between waves. Some snapshots of the computed free surface are depicted in Figure 8. As it can be observed, there are no oscillations at the neighbourhood of the shock waves, which indicates that the limiting approach provides a high overall quality of the computed numerical solution. The solution is depicted alongside a reference solution that has been computed by a first order scheme with $N_x = 20{,}000$ elements.

Note that the small oscillations appearing with the ADER method could be prevented with an ad hoc tuning of the parameters associated with the limiter described in Section 4. Here, we have maintained the same parameters for both approaches to compare both Runge–Kutta and ADER methods.

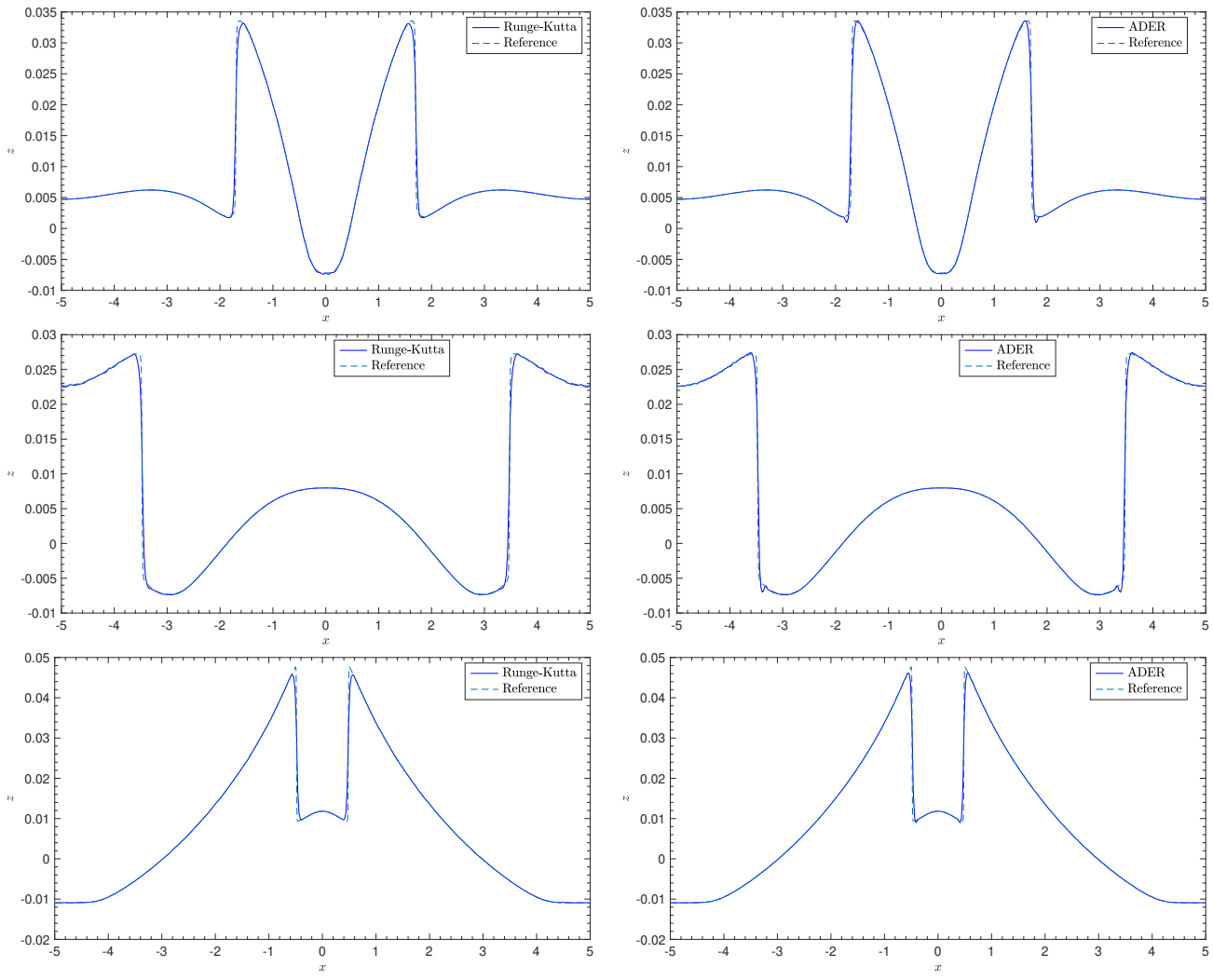

Figure 8. Computed free surface for the problem (54) (shallow water equations) with the fourth-order well-balanced Runge–Kutta (**left**) and ADER (**right**) numerical methods at times $t = 4,\ 5.5,\ 6.5$ s (from upper to lower panels). An uniform Cartesian mesh of $N_x = 400$ elements has been used.

5.3. Compressible Euler Equations with Gravitational Force

We consider the gas dynamic Euler equations written as in (1):

$$U = \begin{pmatrix} \rho \\ \rho u \\ E \end{pmatrix}, \quad F(U) = \begin{pmatrix} \rho u \\ \rho u^2 + p \\ u(E+p) \end{pmatrix}, \quad S(U) = \begin{pmatrix} 0 \\ -\rho \\ -\rho u \end{pmatrix}, \quad G(U) = 0, \tag{55}$$

$\rho \geq 0$ being the density, u the velocity, E the total energy, and $H(x)$ a given continuous gravitational potential. The internal energy e is given by $\rho e = E - \frac{1}{2}\rho u^2$. The pressure $p \geq 0$ is given by e through the equation of state (ideal gas),

$$p = (\gamma - 1)\rho e, \tag{56}$$

where $\gamma > 1$ is the adiabatic constant that will take the value $\frac{5}{3}$ unless stated otherwise.

In this work, we will focus on the hydrostatic steady states solutions given by

$$u = 0, \quad \partial_x p = -\rho H'(x). \tag{57}$$

According to [35], a family of stationary solutions of (55) with $u = 0$ are

$$u = 0, \quad \rho = \alpha(H, C_1) \geq 0, \quad p(x) = \beta(H, C_1, C_2) \geq 0, \quad E = \frac{p(x)}{\gamma - 1}, \tag{58}$$

where α is a given continuous function and β is given by

$$\partial_\sigma \beta(H, C_1, C_2) = -\alpha(H, C1).$$

The numerical methods are then chosen to preserve one of those families given by the choice of α :

$$\alpha(H, C_1) = C_1 e^{-H}, \tag{59}$$

that results in the following set of stationary solutions with $u = 0$,

$$u = 0, \quad \rho = C_1 e^{-H} \geq 0, \quad p = C_1 e^{-H} + C_2 \geq 0, \quad E = \frac{p}{\gamma - 1}. \tag{60}$$

5.3.1. Preserving Stationary Solutions

In this experiment, we set as initial condition a stationary solution of the form (60) to check the well-balancing properties of the proposed methods for the system (55). The initial condition is given by

$$u = 0, \quad \rho = e^{-H}, \quad p(x, 0) = e^{-H}, \quad E = \frac{p}{\gamma - 1}, \quad H = x. \tag{61}$$

The computational domain is $\Omega = [-1, 1]$ and Dirichlet boundary conditions were imposed everywhere. Figure 9 shows the error between the compute numerical solutions and the stationary one given by (61). As it can be seen in Figure 9 and Table 5, the well-balanced methods can preserve the stationary solution at a final time $t = 10$ s.

Table 5. Numerical validation of the well-balanced and non well-balanced methods for the stationary problem (61) (Euler equations). Table contains L_1 errors for the density variable ρ at a final time $t = 10$ s for both Runge–Kutta and ADER DG schemes of order $N + 1 = 1, 2, 3, 4$. Uniform Castesian meshes of N_x elements has been used.

		Non-Well-Balanced		Well-Balanced	
N	N_x	**Runge–Kutta**	**ADER**	**Runge–Kutta**	**ADER**
0		5.13×10^{-02}	1.03×10^{-02}	7.99×10^{-17}	1.31×10^{-16}
		3.18×10^{-02}	5.46×10^{-03}	2.31×10^{-16}	4.42×10^{-16}
		1.77×10^{-02}	3.21×10^{-03}	1.94×10^{-16}	6.21×10^{-16}
		9.41×10^{-03}	1.85×10^{-03}	3.26×10^{-16}	6.61×10^{-16}
1		2.35×10^{-04}	3.08×10^{-04}	7.46×10^{-16}	1.15×10^{-15}
		7.10×10^{-05}	8.81×10^{-05}	1.20×10^{-15}	1.47×10^{-15}
		1.94×10^{-05}	2.34×10^{-05}	2.15×10^{-15}	2.65×10^{-15}
		9.26×10^{-06}	6.03×10^{-06}	3.17×10^{-15}	4.21×10^{-15}
2		3.52×10^{-06}	2.98×10^{-06}	1.06×10^{-15}	2.84×10^{-15}
		5.40×10^{-07}	4.67×10^{-07}	1.78×10^{-15}	5.01×10^{-15}
		7.44×10^{-08}	6.58×10^{-08}	4.40×10^{-15}	9.39×10^{-15}
		9.75×10^{-09}	8.73×10^{-09}	4.93×10^{-15}	1.36×10^{-14}
3		8.20×10^{-09}	1.81×10^{-08}	1.26×10^{-15}	1.35×10^{-14}
		7.14×10^{-10}	1.53×10^{-09}	2.74×10^{-15}	2.83×10^{-14}
		5.18×10^{-11}	1.09×10^{-10}	7.71×10^{-15}	4.53×10^{-14}
		3.48×10^{-12}	7.00×10^{-12}	9.54×10^{-15}	7.16×10^{-14}

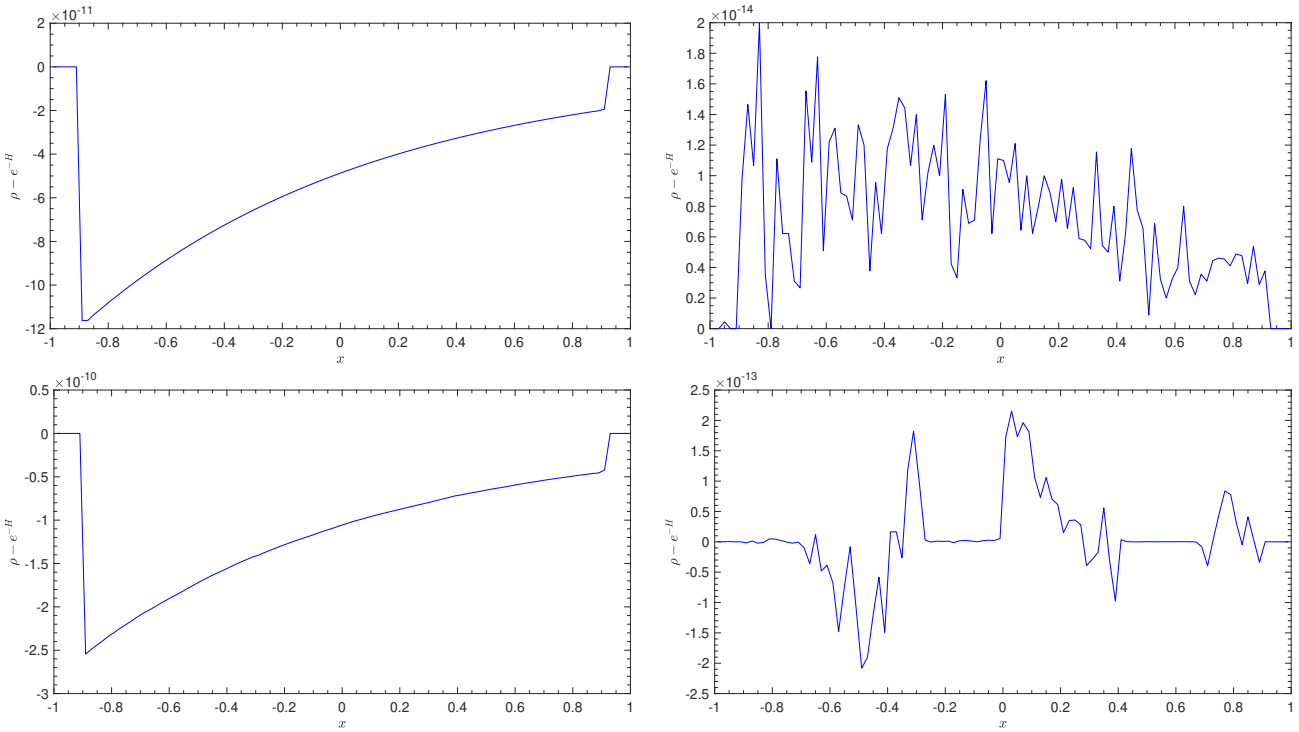

Figure 9. Computed density variable fluctuation $\rho - e^{-H}$ for the stationary problem (61) (Euler equations) at time $t = 10$ s with the fourth order non well-balanced (**left**) and well-balanced (**right**) methods. An uniform Cartesian mesh of $N_x = 100$ elements has been used. Upper and lower panels stands for Runge–Kutta and ADER time-marching discretisations, respectively.

5.3.2. Limited Simulation

We check again the well behaviour of the proposed mixed-order technique described in this paper. To do that, we set $H = 0$, $\gamma = 1.4$, and consider the following discontinuous initial condition given by

$$\begin{cases} \left(\rho_L, \quad u_L, \quad p_L\right) & \text{if } x < 0, \\ \left(\rho_L, \quad u_R, \quad p_L\right) & \text{if } x \geq 0. \end{cases} \tag{62}$$

Then, we set the values for the two well-known numerical tests:

- The sod problem [94]:

$$\left(\rho_L, \quad u_L, \quad p_L\right) = \left(1, \quad 0, \quad 1\right), \left(\rho_R, \quad u_R, \quad p_R\right) = \left(0.125 \quad 0 \quad 0.1\right). \tag{63}$$

- The Lax problem [95]:

$$\left(\rho_L \quad u_L \quad p_L\right) = \left(0.445, \quad 0.698, \quad 3.528\right), \left(\rho_R, \quad u_R, \quad p_R\right) = \left(0.5, \quad 0, \quad 0.571\right). \tag{64}$$

In both cases, the computational domain $\Omega = [-5, 5]$ is covered with $N_x = 300$ elements. The limiter value M defined in (33) is set to 0.01, and the CFL number to 0.5. Free outflow boundary conditions were imposed everywhere.

Figures 10 and 11 show the results with the fourth order Runge–Kutta and ADER DG methods for the Sod and Lax problems respectively. The numerical results are compared against a reference solution that has been computed using a first order method with $N_x = 20{,}000$ elements.

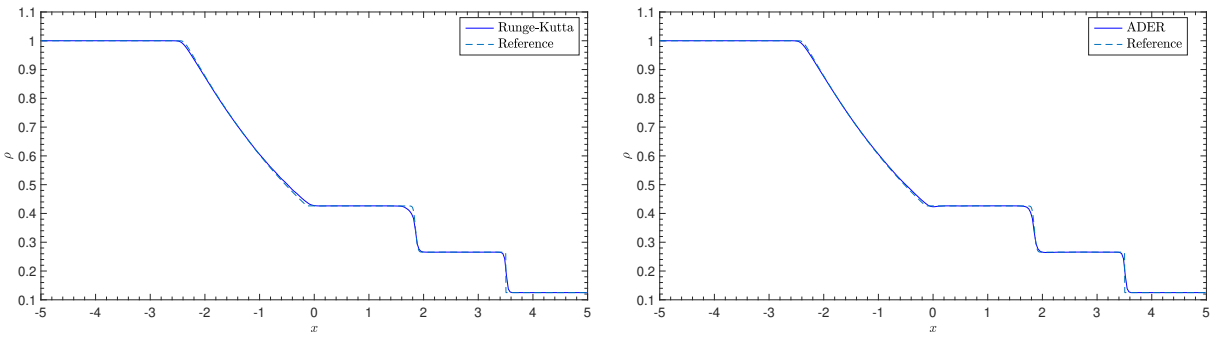

Figure 10. Computed density variable ρ for the problem (63) (Euler equations) with the fourth-order well-balanced Runge–Kutta (**left**) and ADER (**right**) numerical methods at time $t = 2$ s. An uniform Cartesian mesh of $N_x = 300$ elements has been used.

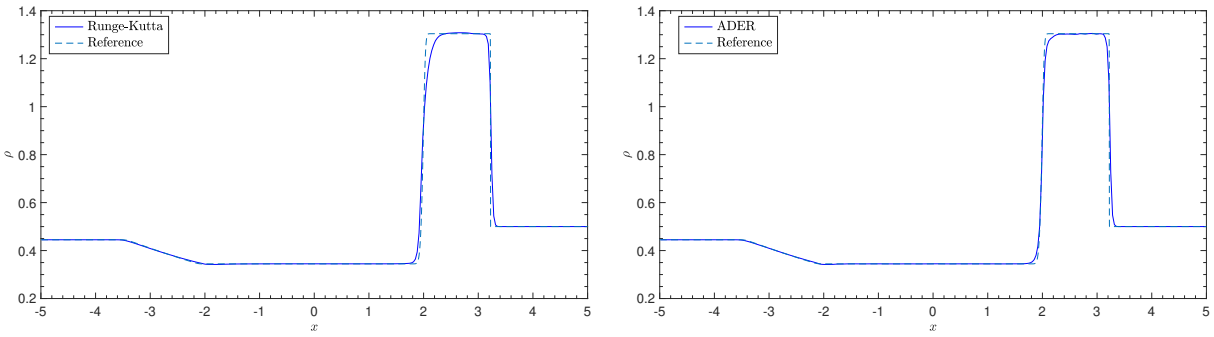

Figure 11. Computed density variable ρ for the problem (64) (Euler equations) with the fourth-order well-balanced Runge–Kutta (**left**) and ADER (**right**) numerical methods at time $t = 1.3$ s. An uniform Cartesian mesh of $N_x = 300$ elements has been used.

5.4. Dispersive Gavrilyuk–Favrie Equations

Finally, we will consider a hyperbolic dispersive shallow water system that was firstly introduced in [96] for the case of a flat bottom bathymetry, and later extended for the non-flat bottom case in [78]. The system can be seen as a hyperbolic relaxation approach of the elliptic Serre–Green–Naghdi equations, and is formally deduced from a master Lagrangian formalism. The system for the case of two-spatial domains reads

$$\partial_t U + \partial_x F_1(U) + \partial_y F_2(U) = S_1(U)\partial_x H + S_2(U)\partial_y H + G(U), \tag{65}$$

where

$$\begin{gathered} U = \begin{pmatrix} h \\ hu \\ hv \\ hw \\ h\xi \end{pmatrix}, \; F_1 = \begin{pmatrix} hu \\ hu^2 + \frac{1}{2}gh^2 + hp \\ uhv \\ uhw \\ uh\xi \end{pmatrix}, \; F_2 = \begin{pmatrix} hv \\ vhu \\ hv^2 + \frac{1}{2}gh^2 + hp \\ vhw \\ vh\xi \end{pmatrix} \\ S_1 = \begin{pmatrix} 0 \\ gh + \frac{3h}{2\xi}p \\ 0 \\ 0 \\ \frac{3}{2}hu \end{pmatrix}, \quad S_2 = \begin{pmatrix} 0 \\ 0 \\ gh + \frac{3h}{2\xi}p \\ 0 \\ \frac{3}{2}hv \end{pmatrix}, \quad G = \begin{pmatrix} 0 \\ 0 \\ 0 \\ \lambda\left(1 - \frac{\xi}{h}\right) \\ hw \end{pmatrix}. \end{gathered} \tag{66}$$

Here, $h = h(x, y, t)$ is the water depth, $H = H(x, y)$ is the known still water depth that we will assume to be continuous, and u, v, w are the depth averaged velocities at the x, y and z direction respectively. Furthermore, $p(h, \xi)$ is the non-hydrostatic pressure

$$p = \frac{3\xi}{h}\left(1 - \frac{\xi}{h}\right),$$

$g = 9.81$ is the gravitational acceleration, and λ is a large pressure constant parameter that makes the system (66) formally converges to the elliptic Serre–Green–Naghdi equations [97] when $\lambda \to \infty$. Finally, $\xi(x, y, t)$ is an auxiliary equilibrium variable introduced in the relaxation procedure. In the following, we will set $\lambda = 300$ for the numerical test considered.

The system satisfied an extra energy conservation law, and the eigenstructure is fully well known. For more details, the reader is refereed to [78]. As for Shallow-water equations, we will consider the family of stationary lake at rest solutions given by

$$u = v = w = 0, \quad \eta = cst, \quad h\xi = h^2, \tag{67}$$

where $\eta = h - H$ is the free-surface elevation.

There are many crucial reasons for considering the numerical validation of the proposed methods for that system here: we will validate the proposed numerical methodology for dispersive shallow flows numerical solutions, and the case of two spatial dimensions; the system introduces a non-homogeneous geometrical source term $G(U)$; the usual steady-states lake at rest solutions for this system contains nonlinear relations between the conserved variables, and that makes standard well-balancing techniques no longer valid to preserve them. Finally, up to our knowledge, this is the first time that a well-balanced high-order method has been proposed for this particular dispersive hyperbolic system.

5.4.1. Preserving Stationary Solutions

In this first numerical experiment, we set as initial condition a stationary solution of the form (67) to check the well-balancing abilities of the proposed methods for the system (66). The initial condition considered (see Figure 12) is given by

$$u = v = w = 0, \quad h = H, \quad h\xi = h^2, \; H = 1 - 0.2e^{-2(x^2+y^2)}. \tag{68}$$

The computational domain is $\Omega = [-5,5] \times [-5,5]$ and periodic boundary conditions are imposed. As it can be seen in Figures 13 and 14 and Table 6, the well-balanced methods are able to preserve the stationary solution at a final time $t = 10$ s for both time-marching discretization and relative coarse meshes. Note that the solutions are compared against the stationary solution (68) as reference.

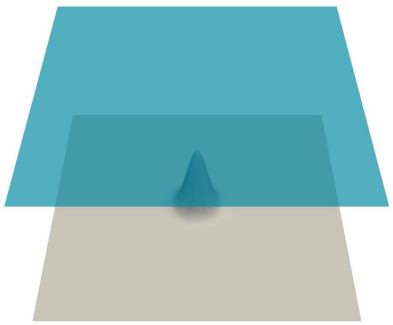

Figure 12. Bottom and the initial lake at rest free surface condition for the stationary problem (68) (dispersive Gavrilyuk–Favrie equations).

Table 6. Numerical validation of the well-balanced and non well-balanced methods for the stationary problem (68) (dispersive Gavrilyuk–Favrie equations). Table contains L_1 errors for the water depth variable h at a final time $t = 10$ s for Runge–Kutta and ADER DG schemes of order $N+1 = 1, 2, 3, 4$. Uniform Cartesian meshes of $N_x \times N_y$ elements has been used.

		Non-Well-Balanced		**Well-Balanced**	
N	$N_x \times N_y$	**Runge–Kutta**	**ADER**	**Runge–Kutta**	**ADER**
0	20×20	8.06×10^{-01}	1.37×10^{01}	0	0
	30×30	5.80×10^{01}	3.72×10^{01}	0	0
	40×40	4.25×10^{-01}	5.36×10^{-01}	0	0
	50×50	2.28×10^{-01}	2.21×10^{-01}	0	0
1	20×20	1.48×10^{-02}	1.71×10^{-02}	0	0
	30×30	4.20×10^{-03}	4.82×10^{-03}	5.30×10^{-15}	3.31×10^{-14}
	40×40	1.75×10^{-03}	2.01×10^{-03}	0	0
	50×50	8.68×10^{-04}	1.02×10^{-03}	1.11×10^{-14}	7.56×10^{-14}
2	20×20	2.38×10^{-03}	2.62×10^{-03}	0	0
	30×30	8.46×10^{-04}	8.85×10^{-04}	2.77×10^{-14}	1.24×10^{-13}
	40×40	3.70×10^{-04}	3.80×10^{-04}	0	0
	50×50	1.87×10^{-04}	1.92×10^{-04}	4.45×10^{-14}	1.97×10^{-13}
3	20×20	3.52×10^{-04}	4.09×10^{-04}	0	0
	30×30	4.30×10^{-05}	4.60×10^{-05}	2.05×10^{-13}	2.76×10^{-13}
	40×40	9.03×10^{-06}	9.75×10^{-06}	1.97×10^{-13}	2.97×10^{-13}
	50×50	2.82×10^{-06}	3.23×10^{-06}	3.57×10^{-13}	3.62×10^{-13}

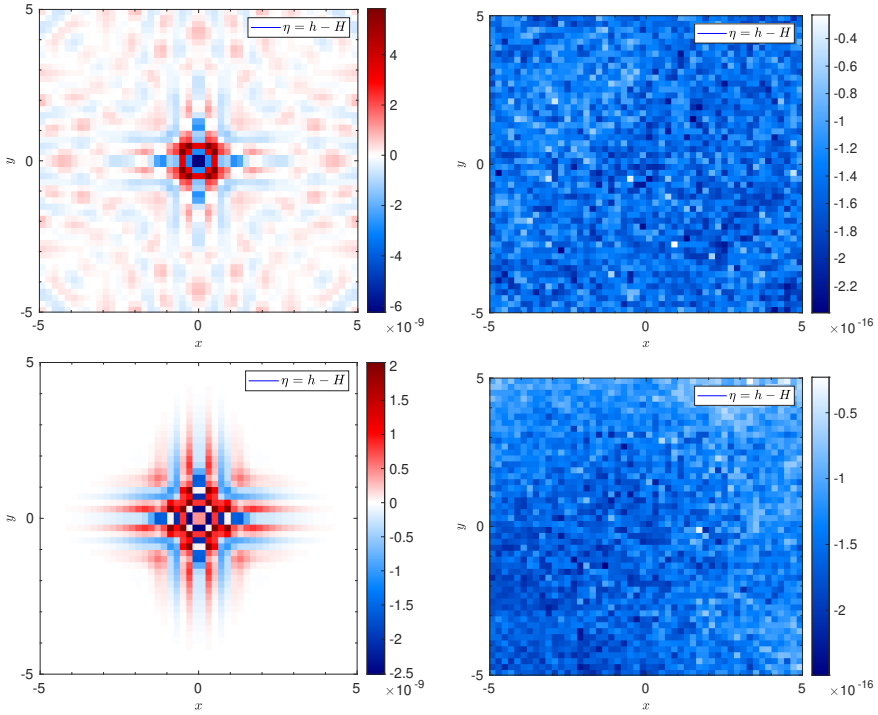

Figure 13. Computed free surface for the stationary problem (68) (dispersive Gavrilyuk–Favrie equations) at time $t = 10$ s with the fourth-order non-well-balanced (**left**) and well-balanced (**right**) methods. A uniform Cartesian mesh of $N_x \times N_y = 50 \times 50$ elements has been used. Upper and lower panels stands for Runge–Kutta and ADER time-marching discretisations, respectively.

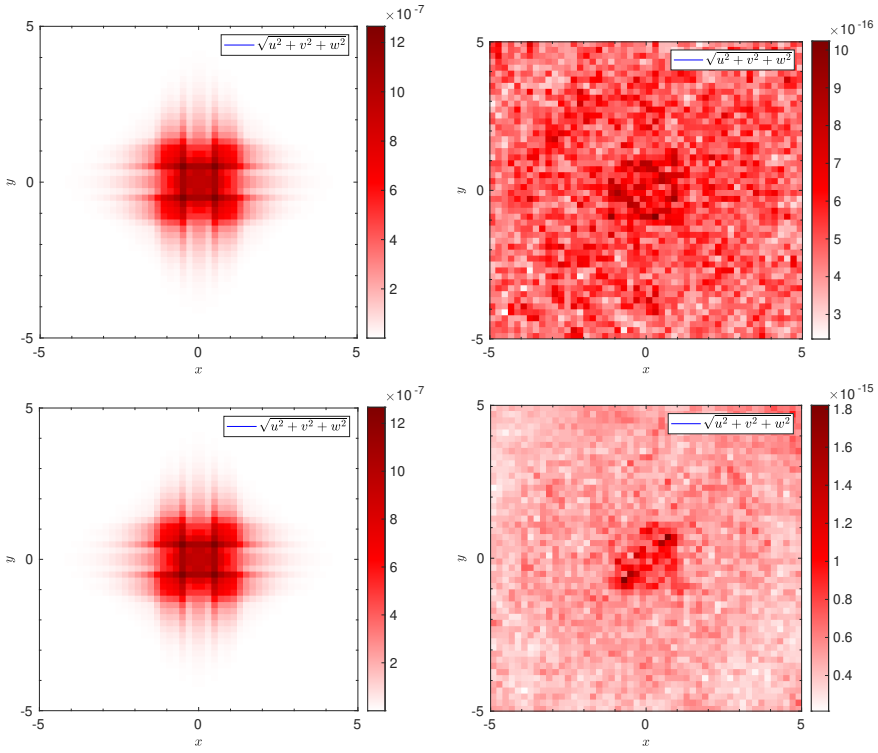

Figure 14. Computed velocity norm $\sqrt{u^2 + v^2 + w^2}$ for the stationary problem (68) (dispersive Gavrilyuk–Favrie equations) at time $t = 10$ s with the fourth order non well-balanced (**left**) and well-balanced (**right**) methods. An uniform Cartesian mesh of $N_x \times N_y = 50 \times 50$ elements has been used. Upper and lower panels stands for Runge–Kutta and ADER time-marching discretisations, respectively.

5.4.2. Limited Simulation

Next, we check the behaviour of the proposed mixed-order technique described in this paper. To do that, we set the following circular dam-break initial condition:

$$u = v = w = 0, \quad h\xi = h^2, \quad H = 1 - 0.2e^{-2x^2},$$

$$h = \begin{cases} H, & \text{for } x^2 + y^2 \geq 1 \\ 0.25 + H, & \text{for } x^2 + y^2 < 1. \end{cases} \tag{69}$$

The computational domain $\Omega = [-5, 5] \times [-5, 5]$ is covered with a mesh of $N_x \times N_y = 200 \times 200$ elements. We set periodic boundary conditions everywhere. Some snapshots of a section at $y = 0$ of the computed free-surface are depicted in Figure 15 with a fourth-order Runge–Kutta time marching discretization. As it can be observed, the comparison between a limited and a non-limited simulation shows that there is no oscillations at the neighbourhood of the dispersive shock waves. Note that the high-oscillatory and over-amplified waves appearing in Figure 15 from the unlimited numerical solution, are not of the nature of this hyperbolic dispersive system.

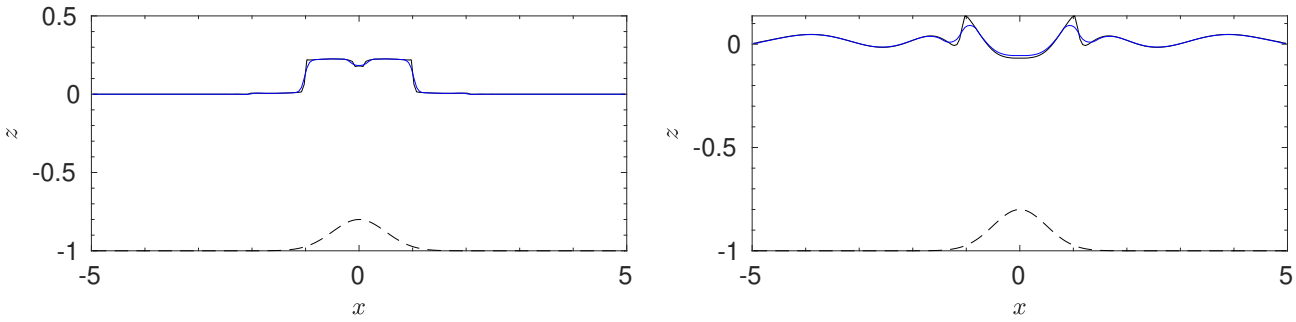

Figure 15. Cross section at $y = 0$ of the computed free-surface for the problem (69) (dispersive Gavrilyuk–Favrie equations) at time $t = 0.1$ s (**left**) and $t = 5$ s (**right**) with the fourth order limited (blue) and non-limited (black) Runge–Kutta DG method. A uniform Cartesian mesh of $N_x \times N_y = 200 \times 200$ elements has been used. Dashed lines stand for the bottom topography H.

6. Conclusions

We have presented a novel and general technique for preserving stationary solutions for Discontinuous Galerkin methods. This general approach is able to transform standard DG schemes in exactly well-balanced arbitrary high-order Discontinuous Galerkin methods for both Runge–Kutta and ADER time-marching discretisations.

For continuous source terms, the methodology only uses a well-suited definition of a well-balanced reconstruction operator and not on the Riemann-solver. Therefore, the well-balanced technique does not rely on the particular details of the system. That makes the method very general and can be applied to any system of hyperbolic PDEs, as long as the desired stationary solutions to be maintained are known.

Furthermore, the standard WENO limiting procedure is carefully considered. Here, we extend classical ideas to propose a novel WENO limiter that preserve stationary solutions. That makes the final numerical methods proposed here arbitrary high-order, essentially non-oscillatory and well-balanced.

We have tested the numerical methodology derived here with some standard systems, proving the well-balancing properties of the approach, the high-order accuracy, and the general well behaviour of the technique in the presence of strong discontinuities.

Author Contributions: Conceptualisation, M.J.C.D., C.E., and E.G.F.; methodology, C.E. and E.G.F.; software, C.E. and E.G.F.; validation, E.G.F. and C.E.; formal analysis, M.J.C.D., E.G.F., and C.E.; investigation, E.G.F., C.E., and M.J.C.D.; resources, M.J.C.D., E.G.F., and C.E.; data curation, C.E. and E.G.F.; writing—original draft preparation, E.G.F. and C.E.; writing—review and editing, M.J.C.D., C.E., and E.G.F.; visualisation, E.G.F. and C.E.; supervision, M.J.C.D.; project administration, M.J.C.D.; funding acquisition, M.J.C.D. All authors have read and agreed to the published version of the manuscript.

Funding: This research has been partially supported by the Spanish Government and FEDER through the coordinated Research project RTI2018-096064-B-C1, the Junta de Andalucía research project P18-RT-3163, the Junta de Andalucia-FEDER-University of Málaga research project UMA18-FEDERJA-16 and the University of Málaga. The University of Málaga has partially supported this research through the "Contrato Puente".

Institutional Review Board Statement: Not applicable.

Informed Consent Statement: Not applicable.

Data Availability Statement: The code and datasets employed in the current paper are available from the authors on reasonable request.

Conflicts of Interest: The authors declare no conflicts of interest.

References

1. Bermúdez, A.; Vázquez, M.E. Upwind methods for hyperbolic conservation laws with source terms. *Comput. Fluids* **1994**, *23*, 1049–1071.
2. Audusse, E.; Bouchut, F.; Bristeau, M.O.; Klein, R.; Perthame, B. A fast and stable well-balanced scheme with hydrostatic reconstruction for shallow water flows. *SIAM J. Sci. Comput.* **2004**, *25*, 2050–2065, doi:10.1137/S1064827503431090.
3. Berberich, J.P.; Chandrashekar, P.; Klingenberg, C. High order well-balanced finite volume methods for multi-dimensional systems of hyperbolic balance laws. *Comput. Fluids* **2021**, *219*, 104858, doi:10.1016/j.compfluid.2021.104858.
4. Guerrero Fernández, E.; Castro-Díaz, M.J.; Luna, T.M.d. A Second-Order Well-Balanced Finite Volume Scheme for the Multilayer Shallow Water Model with Variable Density. *Mathematics* **2020**, *8*, 848.
5. Bermúdez, A.; López, X.; Vázquez-Cendón, M.E. Finite volume methods for multi-component Euler equations with source terms. *Comput. Fluids* **2017**, *156*, 113–134, doi:10.1016/j.compfluid.2017.07.004.
6. Bouchut, F. *Nonlinear Stability of Finite Volume Methods for Hyperbolic Conservation Laws: And Well-Balanced Schemes for Sources*; Springer Science & Business Media: Berlin/Heidelberg, Germany, 2004.
7. Brufau, P.; Vázquez-Cendón, M.; García-Navarro, P. A numerical model for the flooding and drying of irregular domains. *Int. J. Numer. Methods Fluids* **2002**, *39*, 247–275, doi:10.1002/fld.285.
8. Canestrelli, A.; Siviglia, A.; Dumbser, M.; Toro, E.F. Well-balanced high-order centred schemes for non-conservative hyperbolic systems. Applications to shallow water equations with fixed and mobile bed. *Adv. Water Resour.* **2009**, *32*, 834–844, doi:10.1016/j.advwatres.2009.02.006.
9. Castro Díaz, M.J.; Chacón Rebollo, T.; Fernández-Nieto, E.D.; Parés, C. On Well-Balanced Finite Volume Methods for Nonconservative Nonhomogeneous Hyperbolic Systems. *SIAM J. Sci. Comput.* **2007**, *29*, 1093–1126, doi:10.1137/040607642.
10. Chacón Rebollo, T.; Domínguez Delgado, A.; Fernández Nieto, E.D. A family of stable numerical solvers for the shallow water equations with source terms. *Comput. Methods Appl. Mech. Eng.* **2003**, *192*, 203–225, doi:10.1016/S0045-7825(02)00551-0.
11. Chacón Rebollo, T.; Delgado, A.; Fernández-Nieto, E. Asymptotically balanced schemes for non-homogeneous hyperbolic systems - Application to the Shallow Water equations. *Comptes Rendus Math.* **2004**, *338*, 85–90, doi:10.1016/j.crma.2003.11.008.
12. Chandrashekar, P.; Zenk, M. Well-balanced nodal discontinuous Galerkin method for Euler equations with gravity. *J. Sci. Comput.* **2017**, *71*, 1062–1093.
13. Desveaux, V.; Zenk, M.; Berthon, C.; Klingenberg, C. A well-balanced scheme to capture non-explicit steady states in the Euler equations with gravity. *Int. J. Numer. Methods Fluids* **2016**, *81*, 104–127.
14. Desveaux, V.; Zenk, M.; Berthon, C.; Klingenberg, C. Well-balanced schemes to capture non-explicit steady states: Ripa model. *Math. Comput.* **2016**, *85*, 1571–1602.
15. Gaburro, E.; Castro, M.J.; Dumbser, M. Well-balanced Arbitrary-Lagrangian-Eulerian finite volume schemes on moving nonconforming meshes for the Euler equations of gas dynamics with gravity. *Mon. Not. R. Astron. Soc.* **2018**, *477*, 2251–2275, doi:10.1093/mnras/sty542.
16. Gaburro, E.; Castro, M.J.; Dumbser, M. A well balanced diffuse interface method for complex nonhydrostatic free surface flows. *Comput. Fluids* **2018**, *175*, 180–198, doi:10.1016/j.compfluid.2018.08.013.
17. Gaburro, E.; Dumbser, M.; Castro, M.J. Direct Arbitrary-Lagrangian-Eulerian finite volume schemes on moving nonconforming unstructured meshes. *Comput. Fluids* **2017**, *159*, 254–275, doi:10.1016/j.compfluid.2017.09.022.

18. Gosse, L. A well-balanced flux-vector splitting scheme designed for hyperbolic systems of conservation laws with source terms. *Comput. Math. Appl.* **2000**, *39*, 135–159, doi:10.1016/S0898-1221(00)00093-6.
19. Gosse, L. A well-balanced scheme using non-conservative products designed for hyperbolic systems of conservation laws with source terms. *Math. Model. Methods Appl. Sci.* **2001**, *11*, 339–365.
20. Gosse, L. Localization effects and measure source terms in numerical schemes for balance laws. *Math. Comput.* **2002**, *71*, 553–582.
21. Greenberg, J.; Leroux, A.; Baraille, R.; Noussair, A. Analysis and approximation of conservation laws with source terms. *SIAM J. Numer. Anal.* **1997**, *34*, 1980–2007.
22. Greenberg, J.M.; LeRoux, A.Y. A well-balanced scheme for the numerical processing of source terms in hyperbolic equations. *SIAM J. Numer. Anal.* **1996**, *33*, 1–16.
23. Grosheintz-Laval, L.; Käppeli, R. High-order well-balanced finite volume schemes for the Euler equations with gravitation. *J. Comput. Phys.* **2019**, *378*, 324–343, doi:10.1016/j.jcp.2018.11.018.
24. Käppeli, R.; Mishra, S. Well-balanced schemes for the Euler equations with gravitation. *J. Comput. Phys.* **2014**, *259*, 199–219, doi:10.1016/j.jcp.2013.11.028.
25. LeVeque, R.J. Balancing Source Terms and Flux Gradients in High-Resolution Godunov Methods: The Quasi-Steady Wave-Propagation Algorithm. *J. Comput. Phys.* **1998**, *146*, 346–365, doi:10.1006/jcph.1998.6058.
26. Noelle, S.; Pankratz, N.; Puppo, G.; Natvig, J.R. Well-balanced finite volume schemes of arbitrary order of accuracy for shallow water flows. *J. Comput. Phys.* **2006**, *213*, 474–499, doi:10.1016/j.jcp.2005.08.019.
27. Noelle, S.; Xing, Y.; Shu, C.W. High-order well-balanced finite volume WENO schemes for shallow water equation with moving water. *J. Comput. Phys.* **2007**, *226*, 29–58.
28. Pelanti, M.; Bouchut, F.; Mangeney, A. A Roe-type scheme for two-phase shallow granular flows over variable topography. *ESAIM Math. Model. Numer. Anal. Modélisation Mathématique Anal. Numérique* **2008**, *42*, 851–885, doi:10.1051/m2an:2008029.
29. Perthame, B.; Simeoni, C. A kinetic scheme for the Saint-Venant system with a source term. *Calcolo* **2001**, *38*, 201–231, doi:10.1007/s10092-001-8181-3.
30. Perthame, B.; Simeoni, C. Convergence of the upwind interface source method for hyperbolic conservation laws. In *Hyperbolic Problems: Theory, Numerics, Applications*; Springer: Berlin/Heidelberg, Germany, 2003; pp. 61–78.
31. Gómez-Bueno, I.; Castro, M.J.; Parés, C. High-order well-balanced methods for systems of balance laws: A control-based approach. *Appl. Math. Comput.* **2021**, *394*, 125820.
32. Tang, H.; Tang, T.; Xu, K. A gas-kinetic scheme for shallow-water equations with source terms. *Z. Angew. Math. Phys. ZAMP* **2004**, *55*, 365–382.
33. Touma, R.; Koley, U.; Klingenberg, C. Well-balanced unstaggered central schemes for the Euler equations with gravitation. *SIAM J. Sci. Comput.* **2016**, *38*, B773–B807.
34. Müller, L.O.; Parés, C.; Toro, E.F. Well-balanced high-order numerical schemes for one-dimensional blood flow in vessels with varying mechanical properties. *J. Comput. Phys.* **2013**, *242*, 53–85, doi:10.1016/j.jcp.2013.01.050.
35. Castro, M.J.; Parés, C. Well-balanced high-order finite volume methods for systems of balance laws. *J. Sci. Comput.* **2020**, *82*, 48.
36. Parés, C.; Parés-Pulido, C. Well-balanced high-order finite difference methods for systems of balance laws. *J. Comput. Phys.* **2021**, *425*, 109880, doi:10.1016/j.jcp.2020.109880.
37. Reed, W.H.; Hill, T. *Triangular Mesh Methods for the Neutron Transport Equation*; Technical report; Los Alamos Scientific Lab.: Los Alamos, NM, USA, 1973.
38. Cockburn, B.; Hou, S.; Shu, C.W. The Runge-Kutta Local Projection Discontinuous Galerkin Finite Element Method for Conservation Laws. IV: The Multidimensional Case. *Math. Comput.* **1990**, *54*, 545–581.
39. Cockburn, B.; Lin, S.Y.; Shu, C.W. TVB Runge-Kutta local projection discontinuous Galerkin finite element method for conservation laws III: One-dimensional systems. *J. Comput. Phys.* **1989**, *84*, 90–113, doi:10.1016/0021-9991(89)90183-6.
40. Cockburn, B.; Shu, C.W. TVB Runge-Kutta Local Projection Discontinuous Galerkin Finite Element Method for Conservation Laws II: General Framework. *Math. Comput.* **1989**, *52*, 411–435.
41. Cockburn, Bernardo.; Shu, Chi-Wang. The Runge-Kutta local projection P^1-discontinuous-Galerkin finite element method for scalar conservation laws. *ESAIM: M2AN* **1991**, *25*, 337–361, doi:10.1051/m2an/1991250303371.
42. Xing, Y.; Zhang, X.; Shu, C.W. Positivity-preserving high order well-balanced discontinuous Galerkin methods for the shallow water equations. *Adv. Water Resour.* **2010**, *33*, 1476–1493, doi:10.1016/j.advwatres.2010.08.005.
43. Xing, Y. Exactly well-balanced discontinuous Galerkin methods for the shallow water equations with moving water equilibrium. *J. Comput. Phys.* **2014**, *257*, 536–553, doi:10.1016/j.jcp.2013.10.010.
44. Xing, Y.; Shu, C.W. High order finite difference WENO schemes with the exact conservation property for the shallow water equations. *J. Comput. Phys.* **2005**, *208*, 206–227, doi:10.1016/j.jcp.2005.02.006.
45. Xing, Y.; Shu, C.W. High Order Well-Balanced Finite Volume WENO Schemes and Discontinuous Galerkin Methods for a Class of Hyperbolic Systems with Source Terms. *J. Comput. Phys.* **2006**, *214*, 567–598, doi:10.1016/j.jcp.2005.10.005.
46. Xing, Y.; Shu, C.W.; Noelle, S. On the Advantage of Well-Balanced Schemes for Moving-Water Equilibria of the Shallow Water Equations. *J. Sci. Comput.* **2011**, *48*, 339–349.
47. Bollermann, A.; Noelle, S.; Lukacova-Medvidova, M. Finite volume evolution Galerkin methods for the shallow water equations with dry beds. *Commun. Comput. Phys.* **2010**, *10*.

48. Xing, Y.; Zhang, X. Positivity-preserving well-balanced discontinuous Galerkin methods for the shallow water equations on unstructured triangular meshes. *J. Sci. Comput.* **2013**, *57*, 19–41.
49. Li, G.; Xing, Y. Well-balanced discontinuous Galerkin methods for the Euler equations under gravitational fields. *J. Sci. Comput.* **2016**, *67*, 493–513.
50. Li, G.; Xing, Y. Well-balanced discontinuous Galerkin methods with hydrostatic reconstruction for the Euler equations with gravitation. *J. Comput. Phys.* **2018**, *352*, 445–462.
51. Ern, A.; Piperno, S.; Djadel, K. A well-balanced Runge–Kutta discontinuous Galerkin method for the shallow-water equations with flooding and drying. *Int. J. Numer. Methods Fluids* **2008**, *58*, 1–25, doi:10.1002/fld.1674.
52. Vater, S.; Beisiegel, N.; Behrens, J. A limiter-based well-balanced discontinuous Galerkin method for shallow-water flows with wetting and drying: One-dimensional case. *Adv. Water Resour.* **2015**, *85*, 1–13.
53. Gassner, G.J.; Winters, A.R.; Kopriva, D.A. A well balanced and entropy conservative discontinuous Galerkin spectral element method for the shallow water equations. *Appl. Math. Comput.* **2016**, *272*, 291–308.
54. Taube, A.; Dumbser, M.; Balsara, D.S.; Munz, C.D. Arbitrary high-order discontinuous Galerkin schemes for the magnetohydrodynamic equations. *J. Sci. Comput.* **2007**, *30*, 441–464.
55. Dumbser, M.; Munz, C.D. Building blocks for arbitrary high order discontinuous Galerkin schemes. *J. Sci. Comput.* **2006**, *27*, 215–230.
56. Qiu, J.; Dumbser, M.; Shu, C.W. The discontinuous Galerkin method with Lax–Wendroff type time discretizations. *Comput. Methods Appl. Mech. Eng.* **2005**, *194*, 4528–4543, doi:10.1016/j.cma.2004.11.007.
57. Tumolo, G.; Bonaventura, L.; Restelli, M. A semi-implicit, semi-Lagrangian, p-adaptive discontinuous Galerkin method for the shallow water equations . *J. Comput. Phys.* **2013**, *232*, 46–67.
58. Dumbser, M.; Casulli, V. A staggered semi-implicit spectral discontinuous Galerkin scheme for the shallow water equations. *Appl. Math. Comput.* **2013**, *219*, 8057–8077.
59. Tavelli, M.; Dumbser, M. A high order semi-implicit discontinuous Galerkin method for the two dimensional shallow water equations on staggered unstructured meshes. *Appl. Math. Comput.* **2014**, *234*, 623–644.
60. Busto, S.; Tavelli, M.; Boscheri, W.; Dumbser, M. Efficient high order accurate staggered semi-implicit discontinuous Galerkin methods for natural convection problems. *Comput. Fluids* **2020**, *198*, 104399.
61. Titarev, V.; Toro, E. ADER: Arbitrary high order godunov approach. *J. Sci. Comput.* **2002**, *17*, 609–618, doi:10.1023/A:1015126814947.
62. Toro, E.; Titarev, V. Solution of the generalized Riemann problem for advection-reaction equations. *Proc. R. Soc. A Math. Phys. Eng. Sci.* **2002**, *458*, 271–281. cited By 159, doi:10.1098/rspa.2001.0926.
63. Titarev, V.; Toro, E. ADER schemes for three-dimensional non-linear hyperbolic systems. *J. Comput. Phys.* **2005**, *204*, 715 – 736, doi:10.1016/j.jcp.2004.10.028.
64. Toro, E.; Titarev, V. Derivative Riemann solvers for systems of conservation laws and ADER methods. *J. Comput. Phys.* **2006**, *212*, 150 – 165, doi:10.1016/j.jcp.2005.06.018.
65. Dumbser, M.; Enaux, C.; Toro, E.F. Finite volume schemes of very high order of accuracy for stiff hyperbolic balance laws. *J. Comput. Phys.* **2008**, *227*, 3971 – 4001, doi:10.1016/j.jcp.2007.12.005.
66. Dumbser, M.; Balsara, D.S.; Toro, E.F.; Munz, C.D. A unified framework for the construction of one-step finite volume and discontinuous Galerkin schemes on unstructured meshes. *J. Comput. Phys.* **2008**, *227*, 8209 – 8253, doi:10.1016/j.jcp.2008.05.025.
67. Escalante, C.; de Luna, T.M.; Castro, M. Non-hydrostatic pressure shallow flows: GPU implementation using finite volume and finite difference scheme. *Appl. Math. Comput.* **2018**, *338*, 631 – 659.
68. Li, G.; Song, L.; Gao, J. High order well-balanced discontinuous Galerkin methods based on hydrostatic reconstruction for shallow water equations. *J. Comput. Appl. Math.* **2018**, *340*, 546–560, doi:10.1016/j.cam.2017.10.027.
69. Li, G.; Li, J.; Qian, S.; Gao, J. A well-balanced ADER discontinuous Galerkin method based on differential transformation procedure for shallow water equations. *Appl. Math. Comput.* **2021**, *395*, 125848, doi:10.1016/j.amc.2020.125848.
70. Wu, X.; Kubatko, E.J.; Chan, J. High-order entropy stable discontinuous Galerkin methods for the shallow water equations: Curved triangular meshes and GPU acceleration. *Comput. Math. Appl.* **2021**, *82*, 179–199, doi:10.1016/j.camwa.2020.11.006.
71. Dumbser, M.; Castro, M.; Parés, C.; Toro, E.F. ADER schemes on unstructured meshes for nonconservative hyperbolic systems: Applications to geophysical flows. *Comput. Fluids* **2009**, *38*, 1731–1748, doi:10.1016/j.compfluid.2009.03.008.
72. Izem, N.; Seaid, M.; Wakrim, M. A discontinuous Galerkin method for two-layer shallow water equations. *Math. Comput. Simul.* **2016**, *120*, 12–23, doi:10.1016/j.matcom.2015.04.009.
73. Wintermeyer, N.; Winters, A.R.; Gassner, G.J.; Warburton, T. An entropy stable discontinuous Galerkin method for the shallow water equations on curvilinear meshes with wet/dry fronts accelerated by GPUs. *J. Comput. Phys.* **2018**, *375*, 447–480, doi:10.1016/j.jcp.2018.08.038.
74. Higdon, R.L. Discontinuous Galerkin methods for multi-layer ocean modeling: Viscosity and thin layers. *J. Comput. Phys.* **2020**, *401*, 109018, doi:10.1016/j.jcp.2019.109018.
75. Fernández, E.G.; Díaz, M.J.C.; Dumbser, M.; de Luna, T.M. An Arbitrary High Order Well-Balanced ADER-DG Numerical Scheme for the Multilayer Shallow-Water Model with Variable Density. *J. Sci. Comput.* **2021**, *90*, 52, doi:10.1007/s10915-021-01734-2.
76. Escalante, C.; Dumbser, M.; Castro, M. An efficient hyperbolic relaxation system for dispersive non-hydrostatic water waves and its solution with high order discontinuous Galerkin schemes. *J. Comput. Phys.* **2019**, *394*, 385–416.

77. Bassi, C.; Bonaventura, L.; Busto, S.; Dumbser, M. A hyperbolic reformulation of the Serre-Green-Naghdi model for general bottom topographies. *Comput. Fluids* **2020**, *212*, 104716.
78. Busto Ulloa, S.; Dumbser, M.; Escalante, C.; Favrie, N.; Gavrilyuk, S. On high order ADER discontinuous galerkin schemes for first order hyperbolic reformulations of nonlinear dispersive systems. *J. Sci. Comput.* **2021**, *87*, doi:10.1007/s10915-021-01429-8.
79. Dumbser, M.; Zanotti, O.; Loubère, R.; Diot, S. A posteriori subcell limiting of the discontinuous Galerkin finite element method for hyperbolic conservation laws. *J. Comput. Phys.* **2014**, *278*, 47–75, doi:10.1016/j.jcp.2014.08.009.
80. Cockburn, B.; Shu, C.W. The Runge–Kutta Discontinuous Galerkin Method for Conservation Laws V: Multidimensional Systems. *J. Comput. Phys.* **1998**, *141*, 199–224, doi:10.1006/jcph.1998.5892.
81. Biswas, R.; Devine, K.D.; Flaherty, J.E. Parallel, adaptive finite element methods for conservation laws. *Appl. Numer. Math.* **1994**, *14*, 255–283.
82. Burbeau, A.; Sagaut, P.; Bruneau, C.H. A Problem-Independent Limiter for High-Order Runge–Kutta Discontinuous Galerkin Methods. *J. Comput. Phys.* **2001**, *169*, 111–150, doi:10.1006/jcph.2001.6718.
83. Zhong, X.; Shu, C.W. A simple weighted essentially nonoscillatory limiter for Runge–Kutta discontinuous Galerkin methods. *J. Comput. Phys.* **2013**, *232*, 397–415, doi:10.1016/j.jcp.2012.08.028.
84. Qiu, J.; Shu, C.W. Runge–Kutta discontinuous Galerkin method using WENO limiters. *SIAM J. Sci. Comput.* **2005**, *26*, 907–929.
85. Shi, J.; Hu, C.; Shu, C.W. A technique of treating negative weights in WENO schemes. *J. Comput. Phys.* **2002**, *175*, 108–127.
86. Castro, M.; Fernández-Nieto, E. A Class of Computationally Fast First Order Finite Volume Solvers: PVM Methods. *SIAM J. Sci. Comput.* **2012**, *34*, doi:10.1137/100795280.
87. Castro, M.J.; de Luna, T.M.; Parés, C. Well-balanced schemes and path-conservative numerical methods. In *Handbook of Numerical Analysis*; Elsevier: Amsterdam, The Netherlands, 2017; Volume 18, pp. 131–175.
88. Gallardo, J.M.; Schneider, K.A.; Castro, M.J. On a class of two-dimensional incomplete Riemann solvers. *J. Comput. Phys.* **2019**, *386*, 541–567, doi:10.1016/j.jcp.2019.02.034.
89. Castro, M.J.; Gallardo, J.M.; Marquina, A. A class of incomplete Riemann solvers based on uniform rational approximations to the absolute value function. *J. Sci. Comput.* **2014**, *60*, 363–389.
90. Shu, C.W.; Osher, S. Efficient implementation of essentially non-oscillatory shock-capturing schemes. *J. Comput. Phys.* **1988**, *77*, 439–471, doi:10.1016/0021-9991(88)90177-5.
91. Hidalgo, A.; Dumbser, M. ADER schemes for nonlinear systems of stiff advection–diffusion–reaction equations. *J. Sci. Comput.* **2011**, *48*, 173–189.
92. Jackson, H. On the eigenvalues of the ADER-WENO Galerkin predictor. *J. Comput. Phys.* **2017**, *333*, 409–413.
93. Castro Díaz, M.; López-García, J.; Parés, C. High order exactly well-balanced numerical methods for shallow water systems. *J. Comput. Phys.* **2013**, *246*, 242–264, doi:10.1016/j.jcp.2013.03.033.
94. Sod, G.A. A survey of several finite difference methods for systems of nonlinear hyperbolic conservation laws. *J. Comput. Phys.* **1978**, *27*, 1–31, doi:10.1016/0021-9991(78)90023-2.
95. Lax, P.D. Weak solutions of nonlinear hyperbolic equations and their numerical computation. *Commun. Pure Appl. Math.* **1954**, *7*, 159–193, doi:10.1002/cpa.3160070112.
96. Favrie, N.; Gavrilyuk, S. A rapid numerical method for solving Serre–Green–Naghdi equations describing long free surface gravity waves. *Nonlinearity* **2017**, *30*, 2718.
97. Green, A.E.; Naghdi, P.M. A derivation of equations for wave propagation in water of variable depth. *J. Fluid Mech.* **1976**, *78*, 237–246, doi:10.1017/S0022112076002425.